Stochastic Stability Analysis of the Linear Continuous and Discrete PSO Models

Juan Luis Fernández-Martínez and Esperanza García-Gonzalo

***Abstract*—Particle swarm optimization (PSO) can be interpreted physically as a particular discretization of a stochastic damped mass-spring system. Knowledge of this analogy has been crucial to derive the PSO continuous model and to introduce different PSO family members including the generalized PSO (GPSO) algorithm, which is the generalization of PSO for any time discretization step. In this paper, we present the stochastic analysis of the linear continuous and generalized PSO models for the case of a stochastic center of attraction. Analysis of the GPSO second order trajectories is performed and clarifies the roles of the PSO parameters and that of the cost function through the algorithm execution: while the PSO parameters mainly control the eigenvalues of the dynamical systems involved, the mean trajectory of the center of attraction and its covariance functions with the trajectories and their derivatives (or the trajectories in the near past) act as forcing terms to update first and second order trajectories. The similarity between the oscillation center dynamics observed for different kinds of benchmark functions might explain the PSO success for a broad range of optimization problems. Finally, a comparison between real simulations and the linear continuous PSO and GPSO models is shown. As expected, the GPSO tends to the continuous PSO when time step approaches zero. Both models account fairly well for the dynamics (first and second order moments) observed in real runs. This analysis constitutes so far the most realistic attempt to better understand and approach the real PSO dynamics from a stochastic point of view.**

***Index Terms*—Convergence, generalized PSO (GPSO), particle swarm optimization (PSO), stochastic stability analysis.**

I. Introduction: The Particle Swarm Optimization (PSO) Revised

IN THIS PAPER, we refer to the most basic PSO algorithm to solve optimization problems.

1) Individuals, or particles, are represented by vectors whose length is the number of degrees of freedom of the optimization problem. To start with, a population of N_s particles is initialized with random positions ($\mathbf{x}_i^0$) and velocities ($\mathbf{v}_i^0$). A cost function, $c(\mathbf{x}_i)$, is evaluated for each particle i of the swarm. As time advances, the positions and velocities of each particle are updated as a function of its misfit and the misfit of its neighbors. At time-step $k+1$, the algorithm updates positions $\left(\mathbf{x}_i^{k+1}\right)$ and velocities $\left(\mathbf{v}_i^{k+1}\right)$ of the individuals as follows:

$$\mathbf{v}_i^{k+1} = \omega \mathbf{v}_i^k + \phi_1(\mathbf{g}^k - \mathbf{x}_i^k) + \phi_2(\mathbf{l}_i^k - \mathbf{x}_i^k)$$

$$\mathbf{x}_i^{k+1} = \mathbf{x}_i^k + \mathbf{v}_i^{k+1}$$

with

$$\phi_1 = r_1 a_g \quad \phi_2 = r_2 a_l \quad r_1, r_2 \rightarrow U(0,1) \quad \omega, a_l, a_g \in \mathbb{R}.$$

$\mathbf{l}_i^k$ is the best position found so far by the ith particle and $\mathbf{g}^k$ is the global best position on the whole swarm

$$\mathbf{l}_i^k = \mathbf{x}_i^{k_b} : c\left(\mathbf{x}_i^{k_b}\right) = \min_{1 \le j \le k} c\left(\mathbf{x}_i^j\right) \quad i = 1, \ldots N \tag{1}$$

$$\mathbf{g}^k = \mathbf{l}_{i_g}^k : c\left(\mathbf{l}_{i_g}^k\right) = \min_{1 \le i \le N} c\left(\mathbf{l}_i^k\right). \tag{2}$$

k_b represents for each particle, i, the iteration where its minimum misfit is reached, and i_g is the particle of the swam having the minimum global misfit (or the maximum fitness). ϕ_1, ϕ_2, ω are called the global and local accelerations and the inertia constant, and constitute the PSO tuning parameters.

In PSO, each particle of the swarm has two points of attraction: the global best, $\mathbf{g}^k$, and its previous best position, $\mathbf{l}_i^k$. Thus, the algorithm can be interpreted as a two-discrete gradient method with random effects introduced in the global and local acceleration constants, by uniform random numbers r_1, r_2. This algorithm is very intuitive and easy to program.

2) The literature concerning PSO is very large, but the following references are particularly interesting to understand the aim and originalities presented in this paper.
   a) Those referring to PSO convergence properties and deterministic trajectories analysis [1]–[8]. These analyses served to clarify some numerical aspects of the PSO algorithm and to select some promising parameter sets. As a result of these studies, the first order stability region for the PSO turned out to be

Manuscript received July 17, 2009; revised November 21, 2009 and June 8, 2010. Date of publication December 23, 2010; date of current version June 24, 2011. This work was supported by the University of Oviedo, Oviedo, Spain, and by the "Secretaría de Estado de Universidades y de Investigación" of the Spanish Ministry of Science and Innovation, under a one-year sabbatical grant from 2008 to 2009 at the Department of Civil and Environmental Engineering, University of California Berkeley. This work was also supported by the University of California Berkeley, by the Lawrence Berkeley National Laboratory (Earth Science Division), and by the Energy Resources Engineering Department of Stanford University (Stanford Center for Reservoir Forecasting and Smart Field Consortia) from 2009 to 2010.

The authors are with the Department of Mathematics, University of Oviedo, Oviedo 33007, Spain (e-mail: jlfm@uniovi.es; espe@uniovi.es).

Color versions of one or more of the figures in this paper are available online at http://ieeexplore.ieee.org.

Digital Object Identifier 10.1109/TEVC.2010.2053935

$$S_D = \left\{ \left(\omega, \overline{\phi}\right) : |\omega| < 1,\ 0 < \overline{\phi} < 2\left(\omega + 1\right) \right\}. \tag{3}$$

Also, Clerc and Kennedy [4] introduced a constriction factor to avoid PSO instabilities.

b) Those referring to PSO physical analogies [8]–[10], which allowed us to study the PSO dynamics from a physical point of view. These interdisciplinary points of view brought important advances since the PSO algorithm was first proposed based on a sociological analogy.

c) Those referring to the stochastic analysis of the PSO dynamics. Up to our knowledge, very few attempts to understand the behavior of the PSO in the presence of stochasticity have been made [11]–[17]. Also, it is important to note that in most of these approaches stagnation is adopted as a simplification hypothesis.

3) In the PSO algorithm, the following vectorial difference equation is involved for each particle in the swarm:

$$\begin{cases} \mathbf{x}_i^{k+1} + (\phi - \omega - 1)\mathbf{x}_i^k + \omega \mathbf{x}_i^{k-1} = \phi \mathbf{o}_i^k = \phi_1 \mathbf{g}^k + \phi_2 \mathbf{l}_i^k \\ \mathbf{x}_i^0 = \mathbf{x}_{i0} \\ \mathbf{x}_i^1 = \varphi\left(\mathbf{x}_i^0, \mathbf{v}_{i0}\right) \end{cases} \tag{4}$$

where $\phi = \phi_1 + \phi_2$, and $\mathbf{x}_i^0$, $\mathbf{v}_{i0}$ are the initial positions and velocities [8]. The stability of the mean trajectories (or first order stability) depends only on parameters ω, and $\overline{\phi} = \dfrac{a_g + a_l}{2}$. Choosing the $\left(\omega, \overline{\phi}\right)$ parameters on S_D (3), the particle mean trajectories stabilize around

$$\mathbf{o}_i^k = \frac{a_g \mathbf{g}^k + a_l \mathbf{l}_i^k}{a_g + a_l}.$$

The algorithm finds the global minimum of the cost function, called $\min c$, if $\mathbf{o}_i^k$ approaches $\min c$ as time advances and the particles get attracted toward $\mathbf{o}_i^k$. It is important to remark that the particle attractors, $\mathbf{g}^k$ and $\mathbf{l}_i^k$, depend on the particle trajectories history (see 1 and 2). Also, particle coordinates interact via the cost function $c(\mathbf{x})$ through these terms ($\mathbf{g}^k$ and $\mathbf{l}_i^k$).

4) Difference equation (4) can be considered the result of a centered discretization in acceleration

$$\mathbf{x}_i''(\mathbf{t}) \simeq \frac{\mathbf{x}_i(t + \Delta t) - 2\mathbf{x}_i(t) + \mathbf{x}_i(t - \Delta t)}{\Delta t^2} \tag{5}$$

and a regressive schema in velocity

$$\mathbf{x}_i'(t) \simeq \frac{\mathbf{x}_i(t) - \mathbf{x}_i(t - \Delta t)}{\Delta t} \tag{6}$$

in time $t = k \in \mathbb{N}$, applied to the following system of stochastic differential equations:

$$\begin{cases} \mathbf{x}_i''(t) + (1 - \omega)\mathbf{x}_i'(t) + \phi \mathbf{x}_i(t) = \phi_1 \mathbf{g}(t) + \phi_2 \mathbf{l}_i(t) \quad t \in \mathbb{R} \\ \mathbf{x}_i(\mathbf{0}) = \mathbf{x}_{i0} \\ \mathbf{x}_i'(\mathbf{0}) = \mathbf{v}_{i0} \end{cases} \tag{7}$$

adopting a unit discretization time step, $\Delta t = 1$. Model (7) has been addressed as the PSO continuous model and it has been derived from a mechanical analogy [8]: a damped mass-spring system unit mass, damping factor, $1 - \omega$, and stochastic stiffness constant, ϕ. As we will show, particle coordinates interact via the cost function terms $\mathbf{g}(t)$ and $\mathbf{l}_i(t)$. As in the difference equation case (4), the attractors $\mathbf{g}(t)$ and $\mathbf{l}_i(t)$ in the PSO continuous model (7) depend on the history of trajectories.

5) Finally, using the above-mentioned spring analogy, the generalization of PSO (GPSO) for any iteration time and step discretization step has been derived [16]

$$\begin{aligned} &\mathbf{v}_i(t + \Delta t) = (1 - (1 - \omega)\Delta t)\mathbf{v}_i(t) + \phi_1 \Delta t (\mathbf{g}(t) - \mathbf{x}_i(t)) \\ &+\phi_2 \Delta t (\mathbf{l}_i(t) - \mathbf{x}_i(t)), \mathbf{x}_i(t + \Delta t) = \mathbf{x}_i(t) + \Delta t.\mathbf{v}_i(t + \Delta t) \\ &t,\ \Delta t \in \mathbb{R} \\ &\mathbf{x}_i(0) = \mathbf{x}_{i0}\ \ \mathbf{v}_i(0) = \mathbf{v}_{i0}. \end{aligned} \tag{8}$$

It is important to remark that the introduction of parameter Δt makes (8) physically correct with respect to the velocity and trajectory units. Also, the systematic study of PSO and GPSO trajectories and their comparison to their continuous counterparts in terms of attenuation, oscillation, and center attraction was used to select promising PSO parameter areas, and to clarify the success of some parameter sets proposed in [3]–[5], [8], [16], and [17]. It is important to remark that the first and second stability regions for GPSO with $\Delta t = 1$ are the same found also in earlier research works, nevertheless the GPSO result is more general since it describes how the first and second order stability regions tend to the continuous counterparts as Δt goes to zero.

In this paper, we present the stochastic analysis of the linear continuous and generalized PSO models when the local and global best are considered as stochastic processes having their own dynamics. This analysis is important because in previous work devoted to this subject [14]–[16] both attractors were considered static (stagnation) or having a deterministic behavior.

The roadmap and the main originalities of this paper are the following.

1) The first and second order moments dynamical systems for the linear continuous PSO and GPSO are deduced, allowing a full analysis of the first and second order trajectories. The transient analysis of both dynamical systems completes the one shown by Fernández-Martínez and García-Gonzalo [16] for the GPSO case at the steady state.

2) In the linear PSO continuous model the first and second order moments are governed by two systems of first order linear differential equations, while in the linear GPSO case, two different discrete-time affine dynamical systems arise. In both cases, we analyze the effect of the PSO parameters (inertia and accelerations) on the first and second order stability zones. The contribution

of the center of attraction in the first order moments (mean trajectories) is expressed by the mean trajectory of the center of attraction. For the second order moments (variance and temporal covariance between trajectories) this contribution enters via the covariance functions (similarity) between the center of attraction, the trajectories, and their derivatives (in the continuous case) or the trajectories in the near past (in the GPSO case). Interaction between particle coordinates is also studied in both cases and follows a similar pattern (Appendices A and B).

3) For the linear GPSO case, the analysis of the homogeneous (without taking into account the force term effect) second order trajectories is also performed, illustrating numerically their convergence to their continuous counterparts as discretization time step goes toward zero. This analysis completes the one made in the past for the first order trajectories [8], and serves to explain the similarities and differences between the homogeneous second order trajectories associated with well-known PSO parameter sets proposed in the literature [3]–[5]. This analysis also completes the results shown by Fernández-Martínez and García-Gonzalo [17] . In this paper, we introduced a family of PSO members and showed that the homogeneous versions are isomorphic. Also, we showed numerically that the PSO parameter sets with a high success probability lie (for all the family members) close to the limit of second order stability.
4) The analysis of the oscillation center dynamics for different benchmark functions shows that the involved covariance functions are in all the cases similar and of exponential type, even if their shape does depend on the PSO parameters used, on the number of degrees of freedom of the optimization problem, and on the size and type of the search space (symmetric or asymmetric with respect to the global minimum position). This common fact (together with point 3) might explain why PSO performance depends more on the selection of the PSO parameters than on the kind of cost function. It also explains the PSO success for a broad range of engineering and optimization problems [18].
5) Finally, a comparison between transient solutions of continuous PSO, GPSO, and real runs is performed. For this purpose the dynamic of the center of attraction is inferred empirically through previous numerical simulations. The numerical comparisons show that the linear continuous PSO and GPSO account fairly well for the first and second order trajectories observed in the real simulations when the PSO parameters are chosen on the nonoscillating real zone. In zones of higher variability, such as the first order complex eigenvalue zone, the mean trajectories are perfectly matched but the second order moments differ slightly. The second order moments depend greatly on a correct identification of the experimental covariance terms involved on the second order dynamical systems, which becomes a very difficult task on the areas of high variability.

Based on these results we can state that the results shown in this paper constitute a solid mathematical framework to understand PSO from a stochastic point of view.

II. Stochastic Analysis of the Linear PSO Continuous Model

In this section, we apply the well-established theory of stochastic processes [19] to analyze the stability of random vibrations [20] associated with the PSO mass-spring system. Knowledge issued from the analysis of the linear continuous PSO model is very important to properly understand the GPSO dynamics, and to account separately for the role of the PSO parameters and that of the cost function on the first and second order trajectories. In fact, we will show that GPSO transient solutions approach the PSO continuous counterparts as time step decreases to zero, and both match considerably well the trajectories observed in real runs. Although this can be regarded from the computational point of view as an anecdotal question, it gives important insights into the algorithm convergence.

The linear PSO continuous model (7) is a second order stochastic differential equation with randomness effects introduced by the rigidity parameter, ϕ, and by the forcing term, $\phi_1 \mathbf{g}(t) + \phi_2 \mathbf{l}_i(t)$. As stated above, the major assumption made in this model is that $\mathbf{g}(t)$ and $\mathbf{l}_i(t)$ are stochastic processes that have a certain similarity (covariance function) to the trajectory particle trajectory, $x(t)$. For simplicity, these attractors will be called $g(t)$ and $l(t)$ when they referred to a particle coordinate.

Model (7) can be also written as the following stochastic first order system, which is valid for any particle's coordinate in the swarm:

$$\frac{d\mathbf{Y}(t)}{dt} = A\mathbf{Y}(t) + \mathbf{b}(t) \qquad \mathbf{Y}(0) = \begin{pmatrix} x(0) \\ x'(0) \end{pmatrix} \tag{9}$$

where

$$\mathbf{Y}(t) = \begin{pmatrix} x(t) \\ x'(t) \end{pmatrix} \quad A = \begin{pmatrix} 0 & 1 \\ -\phi & \omega - 1 \end{pmatrix}$$
$$\mathbf{b}(t) = \begin{pmatrix} 0 \\ \phi_1 g(t) + \phi_2 l(t) \end{pmatrix}.$$

Interpreted in the mean square sense[1] [19], the mean of the stochastic process $x(t)$, $\mu(t) = E(x(t))$, fulfills the following ordinary differential equation:

$$\begin{aligned} &\mu''(t) + (1-\omega)\mu'(t) + \overline{\phi}\mu(t) \\ &= E(\phi o(t)) = \frac{a_g E(g(t)) + a_l E(l(t))}{2} \quad t \in \mathbb{R} \\ &\mu(0) = E(x(0)) \\ &\mu'(0) = E(x'(0)). \end{aligned} \tag{10}$$

In this development we suppose that ϕ is independent from $x(t)$, and also $\phi_1, g(t)$ and $\phi_2, l(t)$ are independent. This was

[1] Mean square convergence allows to interchange the derivative and the mean operators.

the case in all the experimental simulations we have performed with benchmark functions using the GPSO algorithm.

In the general case, the solution $\mu(t)$ of (10) can be written as

$$\mu(t) = \mu_h(t) + \mu_p(t) \tag{11}$$

where $\mu_h(t)$ is the general solution of the corresponding homogeneous differential equation, and

$$\mu_p(t) = \frac{a_g E(g(t)) + a_l E(l(t))}{a_g + a_l}.$$

This last expression for $\mu_p(t)$ turns out to be $E(o(t))$, where

$$o(t) = \frac{a_g g(t) + a_l l(t)}{a_g + a_l}.$$

This physically means that $E(o(t))$ is the oscillation center for the mean trajectory $\mu(t)$.

Expressions for $\mu_h(t)$ have been presented by Fernández-Martínez *et al.* [8], as a function of the eigenvalues of the characteristic equation associated with (10). Also, the region of first order stability turned out to be

$$S_C = \{(\omega, \overline{\phi}) : \ \omega < 1, \overline{\phi} > 0\} \tag{12}$$

and the parabola

$$\overline{\phi} = \frac{(1-\omega)^2}{4} \tag{13}$$

separates the regions where the first order eigenvalues are complex or real, defining three different zones for the continuous PSO mean trajectories [8].

Also, defining the mean vector, $\mu(t) = \begin{pmatrix} E(x(t)) \\ E(x'(t)) \end{pmatrix}$, the following first order system of differential equations arises from (9):

$$\frac{d\mu(t)}{dt} = A_\mu . \mu(t) + \mathbf{b}_\mu(t) \qquad \mu(0) = \begin{pmatrix} E(x(0)) \\ E(x'(0)) \end{pmatrix} \tag{14}$$

where

$$A_\mu = \begin{pmatrix} 0 & 1 \\ -\overline{\phi} & \omega - 1 \end{pmatrix}$$

$$\mathbf{b}_\mu(t) = \begin{pmatrix} 0 \\ \dfrac{a_g E(g(t)) + a_l E(l(t))}{2} \end{pmatrix} = \begin{pmatrix} 0 \\ \overline{\phi} E(o(t)) \end{pmatrix}.$$

The solution to the first order system (14) can be written as

$$\mu(t) = e^{A_\mu t}\mu(0) + \int_0^t P e^{D(t-\tau)} P^{-1} \mathbf{b}_\mu(\tau) d\tau \tag{15}$$

where $A_\mu = PDP^{-1}$, and $P = [\mathbf{u}_1, \mathbf{u}_2]$, being $\mathbf{u}_1, \mathbf{u}_2$ the eigenvectors of matrix A_μ. Matrix A_μ admits the diagonal form, $D = \begin{pmatrix} \lambda_1 & 0 \\ 0 & \lambda_2 \end{pmatrix}$, in S_C except on (13). Also developing (15), (11) is found. More precisely, the homogeneous solution, $\mu_h(t) = e^{A_\mu t}\mu(0)$, can be expressed in terms of A_μ eigenvalues as follows:

1) $\mu_h(t) = \mathbf{C}_1 e^{\lambda_1 t} + \mathbf{C}_2 e^{\lambda_2 t}$ in the region of real eigenvalues of matrix A_μ;
2) $\mu_h(t) = \mathbf{C}_1 \cos(\beta t + \mathbf{C}_2) e^{\frac{(\omega-1)}{2} t}$ in the complex region, where β is the imaginary part of the complex eigenvalues;
3) $\mu_h(t) = (\mathbf{C}_1 + \mathbf{C}_2 t)\ e^{\frac{(\omega-1)}{2} t}$ in (13).

A. Particular Cases

1) *Global and local best attractors:* (10) can also be used to account for the dynamics of the global and local best attractors. In the first case $x(t) = g(t) = l(t)$ and thus (10) becomes homogeneous

$$\begin{aligned} &\mu_g''(t) + (1-\omega)\mu_g'(t) = 0 \quad t \in \mathbb{R} \\ &\mu_g(0) = g_0 \\ &\mu_g'(0) = v_{g_0}. \end{aligned} \tag{16}$$

The solution of (16) can be written as

$$\mu_g(t) = g_0 + \frac{v_{g_0}}{1-\omega}\left(1 - e^{-t(1-\omega)}\right).$$

$\mu_g(t)$ is an exponential decreasing trajectory if $\omega < 1$, which is one of the conditions for first order stability. This relation explains that the global best is only perturbed by the effect of the inertia term. This effect becomes very important close to the limit of first order stability, $\omega = 1$.

For any local best particle, $l(t)$, (10) becomes

$$\begin{aligned} &\mu_l''(t) + (1-\omega)\mu_l'(t) + \phi_2\mu_l(t) = \phi_2 g(t) \quad t \in \mathbb{R} \\ &\mu_l(0) = l_0 \\ &\mu_l'(0) = v_{l_0}. \end{aligned} \tag{17}$$

Equation (17) tells that particle $l(t)$ has, as oscillation center, the global best particle $g(t)$, and its properties correspond to the trajectory of a particle in the point $\left(\omega, \frac{a_g}{2}\right)$. This also means that the local best particle will exhibit less variability than a mean particle in the swarm.

2) *Exponential decreasing behavior:* in the case where the oscillation center follows a decreasing exponential function of the form $E(o(t)) = e^{-\gamma t}$, then

$$\mu(t) = e^{A_\mu t}\mu(0) + P(D + \gamma I)^{-1}\left(e^{Dt} - e^{-\gamma t} I\right)\mathbf{v}_2$$

where $\mathbf{v}_2$ is the second column vector of P^{-1}.

3) *Center stagnation:* in case of center stagnation, $E(o(t)) = \beta \in \mathbb{R}$, and vector $\mathbf{b}_\mu$ does not depend on t. Then, (15) simplifies to

$$\mu(t) = e^{A_\mu t}\mu(0) + A_\mu^{-1}\left(e^{A_\mu t} - I\right)\mathbf{b}_\mu.$$

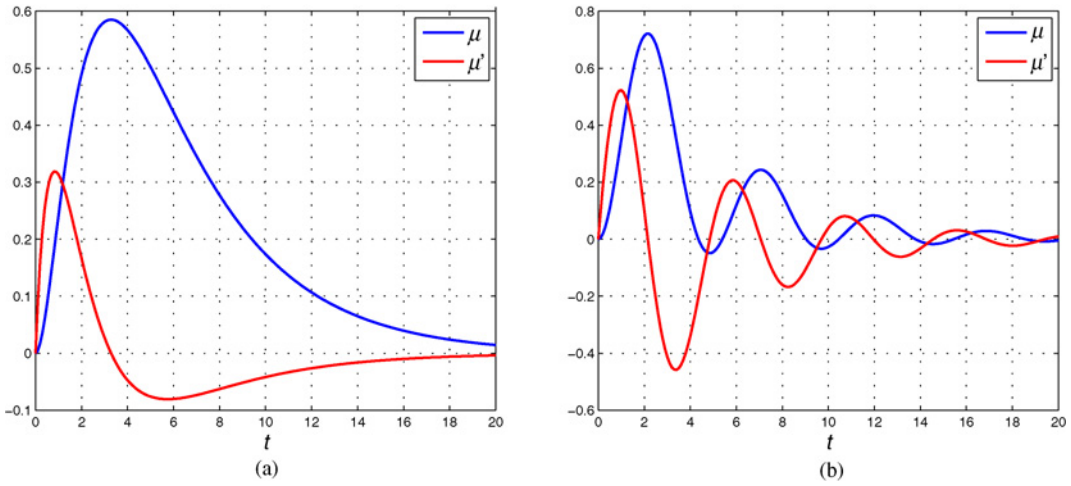

Fig. 1. Transitory solution of the mean differential equation ($\mu(t)$ and $\mu'(t)$) for two different $\left(\omega, \overline{\phi}\right)$ points located on the (a) real zone, $(\omega, \overline{\phi}) = (-1, 0.9)$, and (b) complex zone, $(\omega, \overline{\phi}) = (0.6, 1.7)$, of the first order stability region. In both cases, the oscillation center follows an exponential decreasing trajectory: $\overline{o}(t) = e^{-0.25t}$.

If $E(o(t)) = \beta + e^{-\gamma t}$, solutions for cases 1 and 2 can be superposed, due to the linear character of (14).

4) *Stationary regime:* the stationary regime of the first order system (14) is

$$\mu_s\left(t_p\right) = -A_\mu^{-1}\mathbf{b}_\mu\left(t_p\right) = \begin{pmatrix} \frac{1-\omega}{\overline{\phi}} & \frac{1}{\overline{\phi}} \\ -1 & 0 \end{pmatrix}\begin{pmatrix} 0 \\ \overline{\phi}E\left(o\left(t_p\right)\right) \end{pmatrix} = \begin{pmatrix} E\left(o\left(t_p\right)\right) \\ 0 \end{pmatrix}$$

i.e., choosing the (ω, ϕ) parameters on S_C, the mean trajectory tends to the mean of the oscillation center, and its derivative to zero (center stagnation). This means that the trajectory stabilizes to the center of attraction mean.

Fig. 1 shows for the case of a decreasing exponential behavior with $\beta = 0$, $\gamma = 0.25$, the mean trajectories of stochastic processes $x(t)$ and $x'(t)$ for $\left(\omega, \overline{\phi}\right) = (0.6, 1.7)$ belonging to the complex zone of first order stability region, and $\left(\omega, \overline{\phi}\right) = (-1, 0.9)$ located on the real zone. As it can be observed, the shape of $\mu(t)$ depends on both, the position of the $\left(\omega, \overline{\phi}\right)$ point on the first order stability region, and on the mean trajectory of the oscillation center, named $E(o(t))$.

B. Second Order Moments and the Lyapunov Equation

Let us introduce the noncentered covariance matrix

$$R_{YY} = E\left(\mathbf{Y}\mathbf{Y}^t\right) = \begin{pmatrix} E\left(x^2(t)\right) & E\left(x(t)x'(t)\right) \\ E\left(x(t)x'(t)\right) & E\left(x'^2(t)\right) \end{pmatrix}.$$

The second order moments fulfill the following equations [19], [20]:

$$\frac{dR_{YY}(t)}{dt} = E\left(\mathbf{Y}'\mathbf{Y}^t\right) + E\left(\mathbf{Y}\mathbf{Y}'^t\right)$$

where

$$E\left(\mathbf{Y}'\mathbf{Y}^t\right) = A_\mu E\left(\mathbf{Y}\mathbf{Y}^t\right) + E\left(\mathbf{b}\mathbf{Y}^t\right) = A_\mu R_{YY} + R_{\mathbf{b}Y}$$

$$E\left(\mathbf{Y}\mathbf{Y}'^t\right) = E\left(\mathbf{Y}\mathbf{Y}^t\right)A_\mu^t + E\left(\mathbf{Y}\mathbf{b}^t\right) = R_{YY}A_\mu^t + R_{Y\mathbf{b}}.$$

Then, it is straightforward to show that

$$\frac{dR_{YY}}{dt} = A_\mu R_{YY} + R_{YY}A_\mu^t + R_{\mathbf{b}Y} + R_{Y\mathbf{b}}.$$

This last relation is known in random vibration bibliography as the Lyapunov equation. Developing this expression, we arrive at a linear system of ordinary differential equations

$$\frac{d}{dt}\begin{pmatrix} E\left(x^2(t)\right) \\ E\left(x(t)x'(t)\right) \\ E\left(x'^2(t)\right) \end{pmatrix} = A_\sigma\begin{pmatrix} E\left(x^2(t)\right) \\ E\left(x(t)x'(t)\right) \\ E\left(x'^2(t)\right) \end{pmatrix} + \mathbf{b}_r(t)$$

where

$$A_\sigma = \begin{pmatrix} 0 & 2 & 0 \\ -\overline{\phi} & \omega - 1 & 1 \\ 0 & -2\overline{\phi} & 2(\omega - 1) \end{pmatrix}$$

and

$$\mathbf{b}_r(t) = \begin{pmatrix} 0 \\ E\left(x(t)\left(\phi_1 g(t) + \phi_2 l(t)\right)\right) \\ 2E\left(x'(t)\left(\phi_1 g(t) + \phi_2 l(t)\right)\right) \end{pmatrix}.$$

Under the above mentioned hypothesis of independence

$$E\left(x(t)\left(\phi_1 g(t) + \phi_2 l(t)\right)\right) = \overline{\phi}E\left(x(t)o(t)\right)$$

$$E\left(x'(t)\left(\phi_1 g(t) + \phi_2 l(t)\right)\right) = \overline{\phi}E\left(x'(t)o(t)\right).$$

Thus, $\mathbf{b}_r(t)$ includes the correlation functions between processes $x(t)$, $x'(t)$ and the oscillation center $o(t)$

$$\mathbf{b}_r(t) = \begin{pmatrix} 0 \\ \overline{\phi}E\left(x(t)o(t)\right) \\ 2\overline{\phi}E\left(x'(t)o(t)\right) \end{pmatrix}.$$

It is important to note that $E(u(t)v(t)) = \langle u(t), v(t)\rangle_E$ is the projection of the stochastic process $u(t)$ onto $v(t)$ using

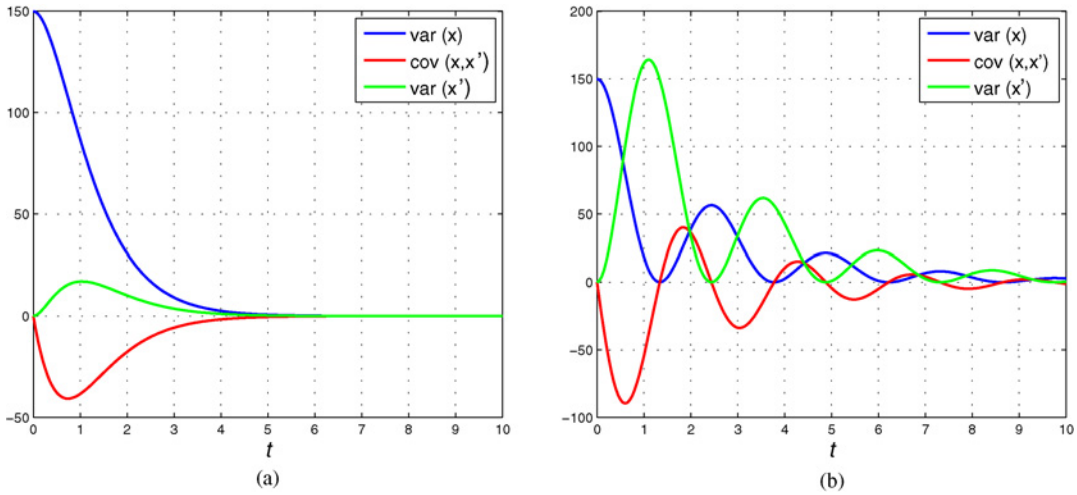

Fig. 2. Homogeneous solution of the covariance equation for the same $(\omega, \overline{\phi})$ points as in Fig. 1, which located on the complex and real zones of the second order stability region. (a) Real zone. (b) Complex zone.

as a scalar product the noncentered covariance (correlation function). Thus, terms involved in $\mathbf{b}_r(t)$ are a measure of the similarity between $x(t)$ and $x'(t)$ to the oscillation center

$$o(t) = \frac{a_g g(t) + a_l l(t)}{a_g + a_l}.$$

Matrix A_σ is regular except for $\overline{\phi} = 0$ and $\omega = 1$, which are the borders of the first order stability region, and has a diagonal form

$$D = \begin{pmatrix} \omega - 1 & 0 & 0 \\ 0 & \omega - 1 - \sqrt{(\omega-1)^2 - 4\overline{\phi}} & 0 \\ 0 & 0 & \omega - 1 + \sqrt{(\omega-1)^2 - 4\overline{\phi}} \end{pmatrix}$$

except on (13). The region of second order stability, in the part of the $(\omega, \overline{\phi})$ plane where the eigenvalues of A_σ are on the unit circle. This region coincides with S_C (12). Also the line separating the zones where the eigenvalues of matrix A_σ are real or complex is (13). This is an important result since, as we will show later in this paper, the dynamics of the GPSO tends to the dynamics of the continuous PSO when the time step Δt goes to zero.

The covariance matrix can then be calculated as follows:

$$\mathbf{C}_{YY} = E\left(\mathbf{Y}\mathbf{Y}^t\right) - \mu\mu^t = R_{YY} - \mu\mu^t$$

where $\mu = \begin{pmatrix} E(x(t)) \\ E(x'(t)) \end{pmatrix}$. Taking into account that

$$\frac{d\mu}{dt} = A_\mu \mu + \begin{pmatrix} 0 \\ \overline{\phi} E(o(t)) \end{pmatrix}$$

then the covariance fulfills

$$\frac{d\mathbf{C}_{YY}}{dt} = A_\mu \mathbf{C}_{YY} + \mathbf{C}_{YY} A_\mu^t + C_{\mathbf{b}Y} + \mathbf{C}_{Y\mathbf{b}} \tag{18}$$

and

$$C_{\mathbf{b}Y} + \mathbf{C}_{Y\mathbf{b}} = \begin{pmatrix} 0 & \overline{\phi}\,\mathrm{Cov}(x(t), o(t)) \\ \overline{\phi}\,\mathrm{Cov}(x(t), o(t)) & 2\overline{\phi}\,\mathrm{Cov}\left(x'(t), o(t)\right) \end{pmatrix}.$$

Introducing the second order vector

$$\sigma(t) = \begin{pmatrix} \mathrm{Var}(x(t)) \\ \mathrm{Cov}\left(x(t), x'(t)\right) \\ \mathrm{Var}\left(x'(t)\right) \end{pmatrix}$$

(18) becomes

$$\begin{aligned} \frac{d\sigma(t)}{dt} &= A_\sigma \sigma(t) + \mathbf{b}_\sigma(t) \\ \sigma(0) &= \sigma_0 \end{aligned} \tag{19}$$

where

$$\mathbf{b}_\sigma(t) = \begin{pmatrix} 0 \\ \overline{\phi}\,\mathrm{Cov}(x(t), o(t)) \\ 2\overline{\phi}\,\mathrm{Cov}\left(x'(t), o(t)\right) \end{pmatrix}$$

and σ_0 stands for the initial conditions for the univariate and bivariate second order moments of $x(t)$ and $x'(t)$. Solution of this first order differential system (18) can be written as follows:

$$\sigma(t) = \sigma_h(t) + \sigma_p(t) = e^{A_\sigma t}\sigma_0 + \int_0^t e^{A_\sigma(t-\tau)}\mathbf{b}_\sigma(\tau)\,d\tau.$$

This expression can be integrated in the same way that the mean equation. More precisely the homogeneous part of $\sigma(t)$, $\sigma_h(t)$, can be expressed as:

1) $\lambda_1, \lambda_2, \lambda_3 \in \mathbb{R}$: $\sigma_h(t) = \mathbf{C}_1 e^{\lambda_1 t} + \mathbf{C}_2 e^{\lambda_2 t} + \mathbf{C}_3 e^{\lambda_3 t}$ in the region of real eigenvalues of matrix A_σ;
2) $\lambda_1 \in \mathbb{R}, \lambda_2, \lambda_3 \in \mathbb{C}$ $\sigma_h(t) = (\mathbf{C}_1 + \mathbf{C}_2 \cos(\beta t + \mathbf{C}_3))e^{(\omega-1)t}$ in the complex region, where β is imaginary part of the complex eigenvalues, λ_2, λ_3;
3) $\lambda_1 = \lambda_2 = \lambda_3 = \omega - 1$: $\sigma_h(t) = \left(\mathbf{C}_1 + \mathbf{C}_2 t + \mathbf{C}_3 t^2\right) e^{(\omega-1)t}$ in (13).

Fig. 2 shows the homogeneous solution, $\sigma_h(t) = e^{A_\sigma t}\sigma_0$, for two points located on the real and complex zones of the second order stability region, S_c.

The stationary solution of the second order moments equation is given by

$$\sigma_s\left(t_p\right) = \begin{pmatrix} \mathrm{Var}\left(x\left(t_p\right)\right) \\ \mathrm{Cov}\left(x\left(t_p\right), x'\left(t_p\right)\right) \\ \mathrm{Var}\left(x'\left(t_p\right)\right) \end{pmatrix} = -A_\sigma^{-1}\mathbf{b}_\sigma\left(t_p\right).$$

Taking into account that

$$A_\sigma^{-1} = \begin{pmatrix} \frac{\overline{\phi}+(\omega-1)^2}{2\overline{\phi}(\omega-1)} & -\frac{1}{\overline{\phi}} & \frac{1}{2\overline{\phi}(\omega-1)} \\ \frac{1}{2} & 0 & 0 \\ \frac{\overline{\phi}}{2(\omega-1)} & 0 & \frac{1}{2(\omega-1)} \end{pmatrix}$$

then

$$\sigma_s\left(t_p\right) = \begin{pmatrix} \mathrm{Cov}\left(x\left(t_p\right), o\left(t_p\right)\right) + \frac{1}{(1-\omega)}\mathrm{Cov}\left(x'\left(t_p\right), o\left(t_p\right)\right) \\ 0 \\ \dfrac{\overline{\phi}}{(1-\omega)}\mathrm{Cov}\left(x'\left(t_p\right), o\left(t_p\right)\right) \end{pmatrix}$$

and taking into account the expression of $\sigma_s\left(t_p\right)$ we can deduce that the second order moments at the steady state are related as follows:

$$\mathrm{Var}\left(x'\left(t_p\right)\right) = \overline{\phi}\left(\mathrm{Var}\left(x\left(t_p\right)\right) - \mathrm{Cov}\left(x\left(t_p\right), o\left(t_p\right)\right)\right)$$

$$\mathrm{Cov}\left(x\left(t_p\right), x'\left(t_p\right)\right) = 0$$

i.e., the stochastic processes $x(t)$ and $x'(t)$ become linearly uncorrelated at steady state t_p.

Finally, the PSO continuous model can also account for the interaction between any two coordinates, i, j, of any two particles in the swarm. Details are provided in Appendix A.

III. Oscillation Center Dynamics

It has been shown that the cost function enters the first and second order moments dynamics through two different forcing terms, including, respectively, the mean trajectory of the center of attraction, $\overline{o}(t)$, and the covariance functions between $x(t)$, $x'(t)$ and $o(t)$. The main conclusion that we reached in this section is that all the experimental functions describing the first and second order moments of the univariate and bivariate distributions of the oscillation center can be fitted using functions of exponential type.

To perform this analysis, we study the typology of these functions by means of numerical experiments with different 1-D benchmark functions [4], [21], [22], having the minimum in $x = 10$, and taking as search space the interval $[0, 30]$. Z1, Z2, and Z3 functions are compositions and combinations [22] of the other functions.

The details of the numerical experiments shown are the following.

1) To perform this numerical analysis we have used two different $\left(\omega, \overline{\phi}\right)$ points with $\Delta t = 1$: $\left(\omega, \overline{\phi}\right) = (0.6, 0.035)$ and $\left(\omega, \overline{\phi}\right) = (0.729, 1.494)$ that are located on the region of second order stability.
2) To calculate the functions describing the univariate and bivariate dynamics of the oscillation center for each of the above mentioned cost functions, we used a swarm of $N_s = 10$ particles evolving during 100 iterations, and we have made $N_r = 3000$ different runs to have at disposal a large statistical sample in each case. Figs. 3 and 4 show the experimental first and second order moments of the oscillation center and its covariance functions with $x(t)$ and $x'(t)$, for the above mentioned 1-D benchmark functions.

The following results are expected.

1) $E(x(t)) \to E(o(t))$. Also, when most of the particles of the swarm converge toward the global optimum, then $E(o(t))$ tends to this point. Fig. 3(a) shows $E(o(t))$ for $\left(\omega, \overline{\phi}\right) = (0.6, 0.035)$ located on the first order real eigenvalue zone, and Fig. 4(a) the same function for the Clerc and Kennedy point, $\left(\omega, \overline{\phi}\right) = (0.729, 1.494)$, which is located on the first order complex eigenvalue zone [4]. It can be observed that the velocity of convergence to the global minimum is greater for this last point. In both cases the Griewank function has the lowest decreasing rate, i.e., the optimization problem with this cost function is the hardest.
2) $\mathrm{Var}(o(t))$ goes to zero with time, i.e., the oscillation center tends to stagnate with iterations. Also, similarity between $\mathrm{Var}(o(t))$ and $\mathrm{Cov}(x(t), o(t))$ increases with time [Figs. 3(b) and 4(b)], as $x(t) \to o(t)$.
   It is important to note that the convergence of the GPSO algorithm to local minima influences the asymptotic value reached by $E(o(t))$ and $\mathrm{Var}(o(t))$.
3) $\mathrm{Cov}(x(t), o(t))$ is a positive function and tends to $\mathrm{Var}(o(t))$ with time, i.e., trajectories are similar to $o(t)$ [Figs. 3(c) and 4(c)].
4) Taking into account that

$$\mathrm{Cov}\left(x'(t), o(t)\right) = \lim_{\Delta t \to 0}\frac{1}{\Delta t}\left(\mathrm{Cov}(x(t), o(t)) - \mathrm{Cov}(x(t-\Delta t), o(t))\right)$$

   then the sign of this function depends on the difference between $\mathrm{Cov}(x(t), o(t))$ and $\mathrm{Cov}(x(t-\Delta t), o(t))$. If the function $\mathrm{Cov}(x(t-\Delta t), o(t))$ is a delayed replica of $\mathrm{Cov}(x(t), o(t))$, then the function $\mathrm{Cov}\left(x'(t), o(t)\right)$ has to be negative, taking into account the positive character of the function $\mathrm{Cov}(x(t), o(t))$. This fact can be observed in real simulations for points located on the real zone [Fig. 3(d)]. For points located on the complex eigenvalue zone [Fig. 4(d)] this function exhibits a greater variability than in the real zone, alternating its sign with time. The "erratic" character of this function on the complex zone will affect greatly the frequency content found on the second order trajectories obtained via the PSO and GPSO dynamical systems, shown later on.

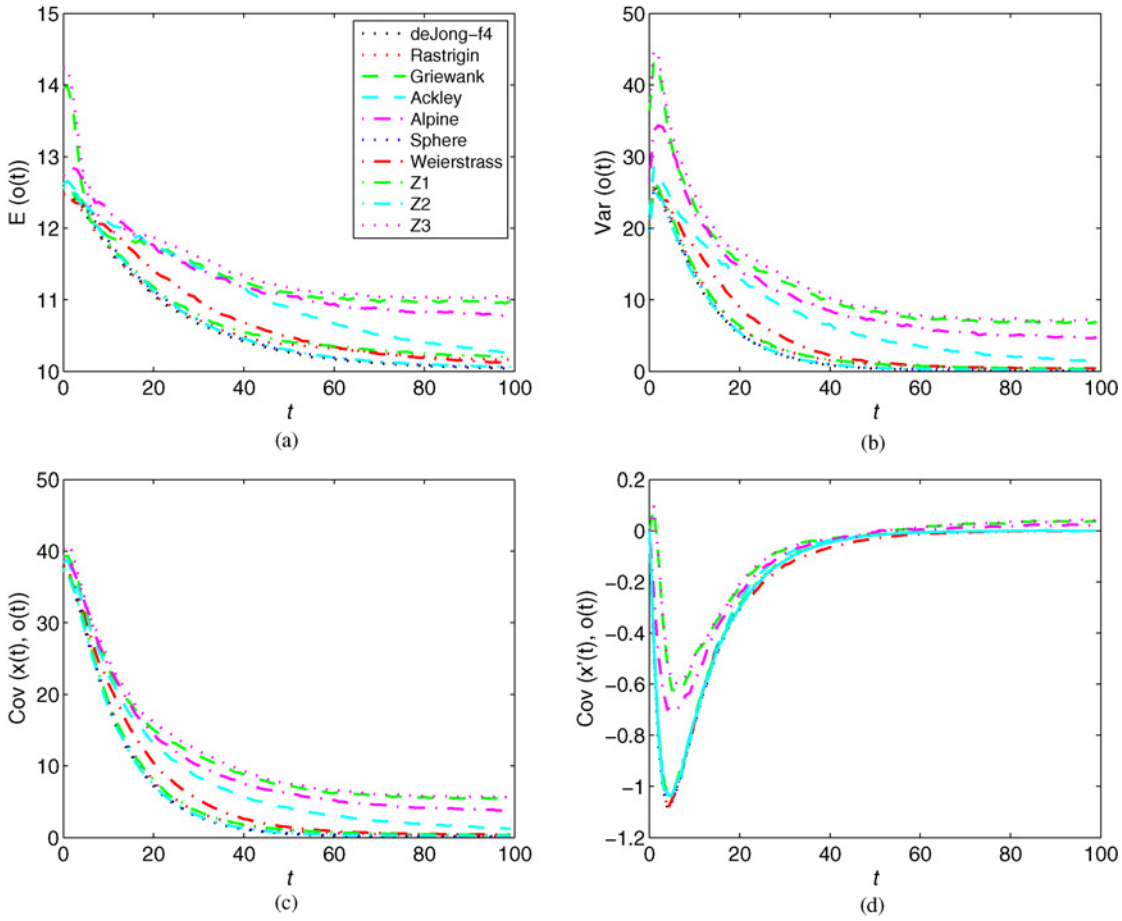

Fig. 3. Trajectories and oscillation center dynamics for different benchmark functions for $(\omega, \overline{\phi}) = (0.6, 0.035)$ and $\Delta t = 1$. Evolution with time. (a) Mean trajectory $E[x(t)]$. (b) Variance of $x(t)$. (c) Covariance between $x(t)$ and $o(t)$. (d) Covariance between $x'(t)$ and $o(t)$.

5) Obviously, the shape of these functions depends on several factors, such as the initial conditions for the first and second order differential systems; on the search space type and on its dimension (number of degrees of freedom of the optimization problem); on the selected PSO parameters; and finally on the type of benchmark function used for optimization. For instance, the initial conditions and the search space might influence the monotonous character of the mean trajectories (decreasing or increasing depending on the situation of the global minimum). Also, when the dimension of optimization problem is increased, or the search space size becomes very broad (no prior knowledge about the global minimum exists), these functions become more erratic at the first iterations, while the PSO algorithm is exploring the search space (Fig. 5). Nevertheless, as we have shown in this section, the results seemed to be very consistent for a wide range of synthetic functions used under the same algorithm conditions. Only the Griewank function seems to have a different behavior which is related to the complexity in finding its global minimum. This circumstance might explain why the PSO algorithm performs acceptably well for a wide range of benchmark functions, and its success depends more on the PSO parameters which have selected for optimization (see [16]). These experimental functions will be used in the last section of this paper to compare second order trajectories issued from the linear continuous PSO, GPSO and real simulations.

IV. Stochastic Analysis of the Linear Generalized PSO

In this section, we first summarize the main results of the GPSO stochastic analysis, first published by Fernández-Martínez and García-Gonzalo [16] for the cases where the global and previous best attractors were considered static (stagnation) or having a deterministic behavior. Second, we extend this analysis to the transient regime in the most general case, i.e., where the center of oscillation exhibits a given stochastic behavior. This analysis is done first for each particle coordinate separately, and afterward we model the interaction between any two particle coordinate trajectories (Appendix B). As for the PSO continuous case, we use a linear version of the GPSO, avoiding the dependence of $\mathbf{g}(t)$ and $\mathbf{l}(t)$ on the visited trajectories.

Finally, we perform an analysis and classification of the GPSO homogeneous second order trajectories which serves

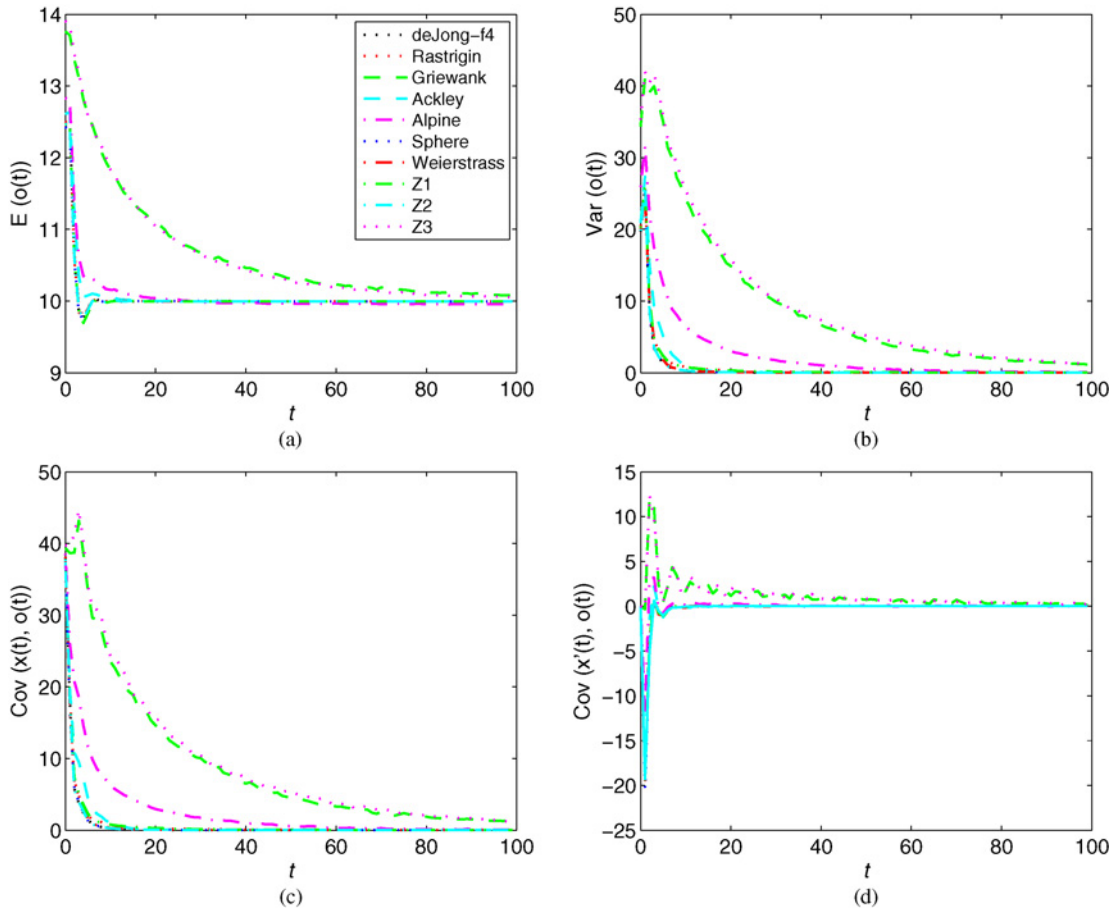

Fig. 4. Trajectories and oscillation center dynamics for different benchmark functions for the Clerc and Kennedy point, $(\omega, \overline{\phi}) = (0.729, 1.494)$ and $\Delta t = 1$. Evolution with time. (a) Mean trajectory $E[x(t)]$. (b) Variance of $x(t)$. (c) Covariance between $x(t)$ and $o(t)$. (d) Covariance between $x'(t)$ and $o(t)$.

us to clarify the role of the inertia, and the local and global accelerations on the second order moments.

A. Linear GPSO Difference Equation

As mentioned above, the generalized PSO arises considering a centered discretization in acceleration, and a regressive schema in velocity in time $t \in \mathbb{R}$, for (7). Considering the PSO continuous model (7), and the above mentioned discretization schemes, (5) and (6), the following second order difference equation is obtained for any time, t, and discretization step, Δt:

$$\mathbf{x}(t + \Delta t) - A\mathbf{x}(t) - B\mathbf{x}(t - \Delta t) = C(t) \quad t, \ \Delta t \in \mathbb{R} \tag{20}$$

where A is a random variable

$$A(\omega, \phi, \Delta t) = 2 - (1 - \omega)\Delta t - \phi \Delta t^2 \tag{21}$$

B is a real constant

$$B(\omega, \Delta t) = (1 - \omega)\Delta t - 1 \tag{22}$$

and

$$C(t) = (\phi_1 \mathbf{g}(t) + \phi_2 \mathbf{l}(t))\Delta t^2 \tag{23}$$

gathers the influence of the global and local best attractors. Difference equation (20) becomes homogeneous when $\Delta t \to 0$.

The stochastic vectorial functional equation (20) corresponds to the so-called GPSO algorithm (8) [16]. GPSO trajectories are modeled as stochastic processes whose univariate and bivariate statistical moments must satisfy the PSO difference equation involved (20). Fernández-Martínez and García-Gonzalo [16] have studied the second order GPSO dynamics at the steady state regime for the case where $g(t)$ and $l(t)$ are considered deterministic functions. Some additional results can be also consulted in [15] for the PSO case ($\Delta t = 1$). In this model, the stochastic behavior of the center of attraction is only due to the effect of random variable ϕ. The stability regions for the first and second order moments turned out to be

$$S_{cr}^1 = \left\{ (\omega, \overline{\phi}) : 1 - \frac{2}{\Delta t} < \omega < 1, \ 0 < \overline{\phi} < \frac{1}{\Delta t^2}(2\omega\Delta t - 2\Delta t + 4) \right\} \tag{24}$$

and

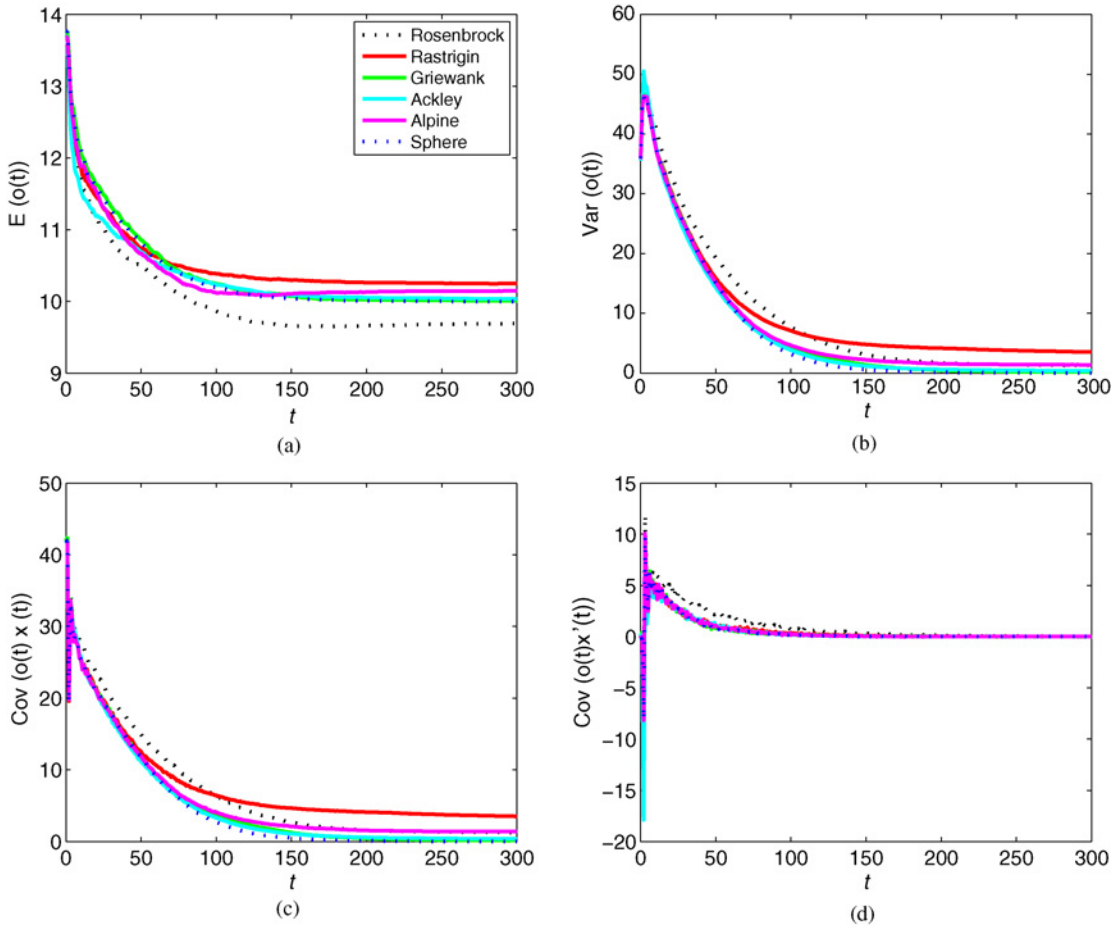

Fig. 5. Trajectories and oscillation center dynamics for different benchmark functions in 30 dimensions for the Clerc and Kennedy's point and $\Delta t = 1$. Evolution with time. (a) Mean trajectory $E[x(t)]$. (b) Variance of $x(t)$. (c) Covariance between $x(t)$ and $o(t)$. (d) Covariance between $x'(t)$ and $o(t)$.

$$S_{cr}^2 = \left\{ \left(\omega, \overline{\phi}\right) : 1 - \frac{2}{\Delta t} < \omega < 1, \;\; 0 < \overline{\phi} < \phi_h\left(\omega, \alpha, \Delta t\right) \right\} \tag{25}$$

where $\phi_h(\omega, \alpha, \Delta t)$ is the hyperbola of second order stability

$$\phi_h(\omega, \alpha, \Delta t) = \frac{12}{\Delta t} \frac{(1-\omega)(2+(\omega-1)\Delta t)}{4-4(\omega-1)\Delta t + \left(\alpha^2 - 2\alpha\right)(2+(\omega-1)\Delta t)} \tag{26}$$

and $\alpha = \dfrac{a_g}{\overline{\phi}} = \dfrac{2a_g}{a_g + a_l}$, is the ratio between the global acceleration and the total mean acceleration. Second order stability region (S_{cr}^2) is inside of the first order stability region (S_{cr}^1) and reaches its maximum size if $\alpha = 1 \;\; \left(a_l = a_g\right)$. Regions of stability for the third and four order moments are imbedded also on the second order stability regions. This result has also been proved by Poli [15] for the PSO case ($\Delta t = 1$). Fernández-Martínez and García-Gonzalo [16] have also shown that temporal covariance between trajectories, $x(t + \Delta t)$ and $x(t)$, at steady state, is zero on the median line of the first order stability triangle, and parameter sets with a high percentage of success are close to the intersection of the median line and the hyperbola $\overline{\phi} = \phi_h$. First and second order stability regions approach the continuous stability region, (12), as time step Δt goes to zero.

B. Stochastic Center of Attraction

In this section we extend the stochastic analysis to the transient case, considering that the oscillation center $o(t)$ as a stochastic process having given covariance functions with the trajectories $x(t)$ and $x(t - \Delta t)$. Also we make the same independence assumptions as in the continuous case. This development allows us to classify the PSO second order trajectories and to provide a better understanding about the PSO parameter tuning.

1) *First Order Trajectories:* Let us call $\mu(t + \Delta t) = \begin{pmatrix} E(x(t+\Delta t)) \\ E(x(t)) \end{pmatrix}$ the vector containing the mean trajectories of $x(t + \Delta t)$ and $x(t)$. The following first order linear system is involved:

$$\mu(t + \Delta t) = \begin{pmatrix} E(A) & B \\ 1 & 0 \end{pmatrix} \mu(t) + \mathbf{d}_\mu(t) \tag{27}$$

where

$$\mathbf{d}_\mu(t) = \begin{pmatrix} \Delta t^2 E(\phi_1 g(t) + \phi_2 l(t)) \\ 0 \end{pmatrix} \overset{ind.}{=} \begin{pmatrix} \overline{\phi} \Delta t^2 E(o(t)) \\ 0 \end{pmatrix}$$

and A, B are given, respectively, by (21) and (22). To deduce (27) we also have supposed the independence between ϕ and $x(t)$, ϕ_1 from $g(t)$, and ϕ_2 and $l(t)$.

The first order stability region turns out also to be (24). Also, supposing that Δt stays invariable through the GPSO algorithm execution, the first order trajectories can be written as

$$\mu(n\Delta t) = A_\mu^n \mu(0) + \sum_{k=1}^{n} A_\mu^{n-k} \mathbf{d}_\mu((k-1)\Delta t).$$

2) *Second Order Moments:* The noncentered second order vector

$$\mathbf{r}_2(t) = \begin{pmatrix} E\left(x^2(t)\right) \\ E(x(t)x(t-\Delta t)) \\ E\left(x^2(t-\Delta t)\right) \end{pmatrix}$$

follows the following second order affine dynamical system:

$$\mathbf{r}_2(t+\Delta t) = A_\sigma \mathbf{r}_2(t) + \mathbf{d}_\mathbf{r}(t) \tag{28}$$

where

$$A_\sigma = \begin{pmatrix} E\left(A^2\right) & 2BE(A) & B^2 \\ E(A) & B & 0 \\ 1 & 0 & 0 \end{pmatrix}$$

and

$$\mathbf{d}_\mathbf{r}(t) = \begin{pmatrix} E\left(C^2(t)\right) + 2BE(C(t)x(t-\Delta t)) + 2E(AC(t)x(t)) \\ \overline{\phi}\Delta t^2 E(o(t)x(t)) \\ 0 \end{pmatrix}.$$

The term $E\left(C^2(t)\right)$ includes the variabilities due to $\phi_1, \phi_2, l(t)$, and $g(t)$

$$\begin{aligned} E\left(C^2(t)\right) &= \Delta t^4 \left(\frac{a_g^2}{3} E\left(g^2(t)\right) + \frac{a_l^2}{3} E\left(l^2(t)\right) \right. \\ &\quad \left. + \frac{a_g a_l}{2} E(l(t)g(t)) \right) \end{aligned}$$

which is related to the variability of the center of attraction

$$\begin{aligned} E\left(o^2(t)\right) &= \frac{1}{\left(a_g + a_l\right)^2} \left(a_g^2 E\left(g^2(t)\right) + a_l^2 E\left(l^2(t)\right) \right. \\ &\quad \left. + 2a_g a_l E(l(t)g(t)) \right) \end{aligned}$$

as follows:

$$E\left(C^2(t)\right) = \frac{\Delta t^4}{3}\left(a_g + a_l\right)^2 \left(E\left(o^2(t)\right) - \frac{a_g a_l}{2} E(l(t)g(t)) \right).$$

The other two terms include the correlations between $x(t)$ and $x(t-\Delta t)$ and the attractors $l(t)$ and $g(t)$

$$2BE(C(t)x(t-\Delta t)) = 2B\Delta t^2 \overline{\phi} E(o(t)x(t-\Delta t))$$

$$\begin{aligned} E(AC(t)x(t)) &= (2-(1-\omega)\Delta t)\overline{\phi} E(o(t)x(t)) \\ &\quad - \Delta t^2 E(\phi C(t)x(t)) \end{aligned}$$

where

$$\begin{aligned} E(\phi C(t)x(t)) &= \Delta t^2 \left(\left(\frac{a_g^2}{3} + \frac{a_g a_l}{4} \right) E(g(t)x(t)) \right. \\ &\quad \left. + \left(\frac{a_l^2}{3} + \frac{a_g a_l}{4} \right) E(l(t)x(t)) \right). \end{aligned}$$

Thus, the analysis of the transient trajectories of second order moments involves the knowledge of the following second order terms.

1) $E\left(g^2(t)\right)$, $E\left(l^2(t)\right)$, $E(l(t)g(t))$.
2) $E(x(t)g(t))$, $E(x(t)l(t))$.
3) $E(x(t-\Delta t)g(t))$, $E(x(t-\Delta t)l(t))$.

Taking (27) and (28) into account, then it is possible to show that the centered second order vector

$$\sigma_\mathbf{2}(\mathbf{t}+\Delta\mathbf{t}) = \begin{pmatrix} \mathrm{Var}(x(t)) \\ \mathrm{Cov}(x(t), x(t-\Delta t)) \\ \mathrm{Var}(x(t-\Delta t)) \end{pmatrix}$$

follows the system

$$\sigma_2(t+\Delta t) = A_\sigma \sigma_2(t) + \mathbf{d}_\mathbf{c}(t) \tag{29}$$

where

$$\begin{aligned} \mathbf{d}_\mathbf{c}(t) &= \mathbf{d}_\mathbf{r}(t) + A_\sigma \begin{pmatrix} \mu^2(t) \\ \mu(t-\Delta t)\mu(t) \\ \mu^2(t-\Delta t) \end{pmatrix} \\ &\quad - \begin{pmatrix} \mu^2(t+\Delta t) \\ \mu(t+\Delta t)\mu(t) \\ \mu^2(t) \end{pmatrix}. \end{aligned}$$

The second order stability region also turns out to be (25). Supposing that Δt stays invariable through the GPSO algorithm execution, the second order trajectories are

$$\sigma_2(n\Delta t) = A_\sigma^n \sigma_2(0) + \sum_{k=1}^{n} A_\sigma^{n-k} \mathbf{d}_\mathbf{c}((k-1)\Delta t). \tag{30}$$

The stationary regimen of second order moments corresponds to the fixed point of dynamical system (29). It is possible to show that over the median line of the first order stability triangle

$$\overline{\phi} = \frac{2 + (\omega - 1)\Delta t}{\Delta t^2}$$

temporal covariance simplifies to

$$\mathrm{Cov}(x(t+\Delta t), x(t)) = E(x(t)o(t)) - E^2(o(t))$$

that goes to zero when center stabilizes. This property of the median line of the stability triangle (first order stability region) has also been cited in Fernández-Martínez and García-Gonzalo [16] for the case where the local and global attractors, $l(t)$ and $g(t)$, are modeled as deterministic functions.

As in the continuous case, the GPSO model can also be used to account for the interaction between any two coordinates of any particle in the swarm. Details are provided in Appendix B.

C. PSO Second Order Trajectories and the PSO Parameter Tuning

In this section, we first analyze the GPSO second order trajectories (variance and covariance) when $\mathbf{d_c}(t) = \mathbf{0}$. Analysis of the homogeneous first order trajectories has been already systematically done in [8]. This analysis allows us to study the contribution of the GPSO parameters (homogeneous parts) from those of the forcing terms (influence of the cost function), on the GPSO second order trajectories.[2] Based on this analysis we explain which are the similarities and difference between the most popular points presented in the literature and we are able to state some general recommendations about how to tune the PSO parameters.

Analysis of eigenvalues of iteration matrix A_σ allows us to study and classify the second order homogeneous trajectories as a function of ω, a_g, a_l, and time step Δt. Solutions of the dynamical system

$$\sigma_2(t+\Delta t) = A_\sigma\left(\omega, a_g, a_l, \Delta t\right).\sigma_2(t)$$

can be expanded in terms of A_σ eigenvalues $(\lambda_1, \lambda_2, \lambda_3)$ and eigenvectors $B_v = \{\mathbf{v}_1, \mathbf{v}_2, \mathbf{v}_3\}$

$$\sigma_2(n\Delta t) = P\begin{pmatrix} \lambda_1^n & 0 & 0 \\ 0 & \lambda_2^n & 0 \\ 0 & 0 & \lambda_3^n \end{pmatrix} P^{-1}\sigma_2(0) = \sum_{i=1}^{3} c_i \lambda_i^n \mathbf{v}_i$$

where $\mathbf{c} = (c_1, c_2, c_3)$ are the coordinates of initial conditions $\sigma_2(0)$ expressed on basis B_v. This implies that variance and covariance trajectories will depend on the kind of A_σ eigenvalues.

This analysis is similar to that shown for the PSO continuous model. If the eigenvalue moduli are less than one in absolute value:

1) When the eigenvalues are real and positive the trajectories are monotonous decreasing.
2) When the eigenvalues are complex, the second order trajectories are oscillatory. Also, negative real eigenvalues or complex eigenvalues with a negative real part originate zigzagging on the second order trajectories.

GPSO second order trajectories depend on ω, a_g, a_l, and Δt. To illustrate this fact, Fig. 6 shows the spectral radius of matrix A_σ [16] and the frequency of the oscillation for the PSO case ($\Delta t = 1$) and $\alpha = 1$ $\left(a_g = a_l\right)$.

In the frequency plot the following zones are clearly differentiated, depending on the character of the A_σ eigenvalues.

1) The real region, which is composed of two different parts: the zigzagging and the exponential decreasing zones. In the zigzagging zone the frequency of the oscillation is $\frac{1}{2}$, and is associated to the presence of negative real eigenvalues.
2) The complex region is composed also of two different non-overlapping zones which are separated by the line of temporal uncorrelation between trajectories (median of the first order stability triangle). The frequency in the complex zone increases from $\overline{\phi} = 0$ and from the upper border of second order stability, toward the limit with the zigzagging real zone.

[2]Although it is clear that the force term also includes the effect of the global and local accelerations.

TABLE I
SPECTRAL RADIUS AND FREQUENCY FOR SECOND ORDER TRAJECTORIES ASSOCIATED TO SOME POPULAR PSO PARAMETER SETS FOUND IN THE LITERATURE

Point	α	$\rho(A_\sigma)$	f (Hz)
Carlisle-Dozier	0.64	0.975	0.463
Clerc-Kennedy	1	0.943	0.462
Trelea	1	0.889	0.5

In this plot, we also show the location of two performance parameter sets found in the literature [4] and [5]. It can be observed that Clerc-Kennedy's point lies on the complex zone, and Trelea's point on the zigzagging zone. Carslile and Dozier's point [3] also lies on the complex zone of A_σ, but in this case $\alpha = 0.64$ $\left(a_l \simeq 2a_g\right)$. Fig. 7 shows the spectral radius of matrix A_σ and the frequency of the oscillation for the PSO case when $\alpha = 0.64$, together with the location of the Carlisle and Dozier's point on the complex eigenvalue zone, very close to the zigzagging region. It can be also observed that the region on second order stability shifts toward lower acceleration values. Table I summarizes the spectral radius and frequency information for these three points.

Trelea's point has the higher frequency $\left(\frac{1}{2}\right)$ and the lowest spectral radius (0.889). Carlisle and Dozier's and Clerc and Kennedy's points have approximately the same frequency (0.463), but Carlisle and Dozier's point has a higher second order spectral radius. This feature implies a higher exploratory capacity for the Carlisle and Dozier's point.

Fig. 8 shows the first and second order trajectories for these three points, compared to the point I, of intersection between the median line of the triangle of convergence and the hyperbola of second order stability for $\alpha = 1$, $\left(\omega, \overline{\phi}\right) = \left(\frac{5}{7}, \frac{12}{7}\right)$. We also show the second trajectories for point II, $\left(\omega, \overline{\phi}\right) = (0.70, 1.70)$, located on the median line below the second order stability region.

The following can be observed.

1) The mean trajectories are similar in all the five cases. In fact, the Clerc and Kennedy's and Carlisle and Dozier's points have the same mean trajectory, because first order trajectories only depend on $\overline{\phi}$ and not on α.
2) The variance associated to Carlisle and Dozier's point is much higher than Clerc and Kennedy's point, even though they have the same mean acceleration, $\overline{\phi}$. Both points belong to the second order complex eigenvalue zone. Trelea's point has the lowest variance and belongs to the second order zigzagging zone. Point I has the greatest variance because it is located on the limit of the second order stability region. Variance for this point does not attenuate with time and stabilizes on 0.336. It can observed that variance for point II lies between that of Carlisle and Dozier's point, and variance of point I.
3) The temporal covariances between trajectories, $\mathrm{Cov}(x(t), x(t-\Delta t))$, for the Trelea's point and for

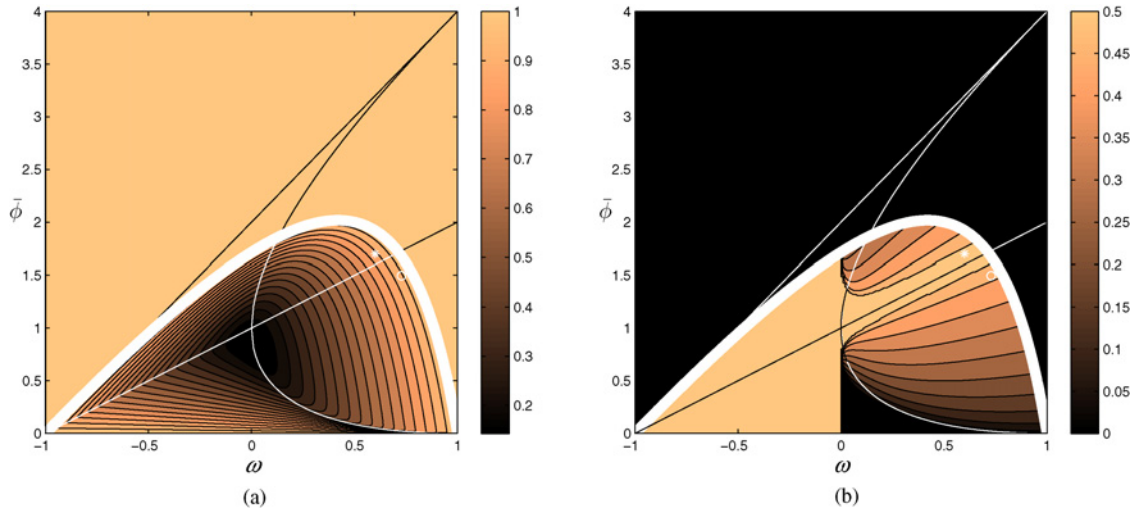

Fig. 6. GPSO. Second order trajectories: spectral radius and frequency as a function of $(\omega, \bar{\phi})$ for $\alpha = 1$ ($a_g = a_l$) and $\Delta t = 1$. Trelea (asterisk) and Clerc and Kennedy (circle) points are also located on these plots. (a) Spectral radius ($\alpha = 1$). (b) Frequency ($\alpha = 1$).

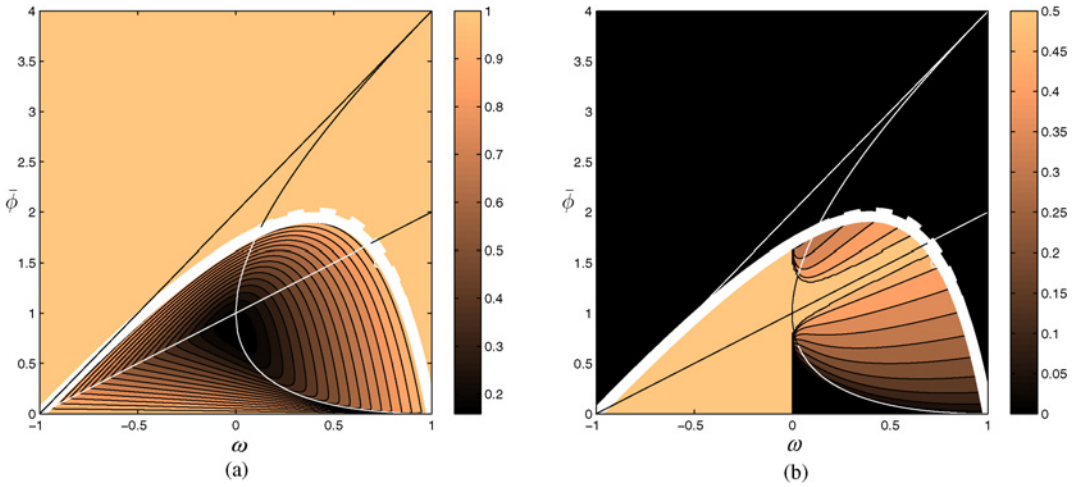

Fig. 7. GPSO. Second order trajectories: spectral radius and frequency as a function of $(\omega, \bar{\phi})$ for $\alpha = 0.64$ ($a_l \simeq 2a_g$) and $\Delta t = 1$. Carlisle and Dozier point (circle) is located on these plots. It can be observed that the upper border of the second order stability region for $\alpha = 0.64$ is nested on the second order stability region for $\alpha = 1$ (pointed hyperbola). (a) Spectral radius ($\alpha = 0.64$). (b) Frequency ($\alpha = 0.64$).

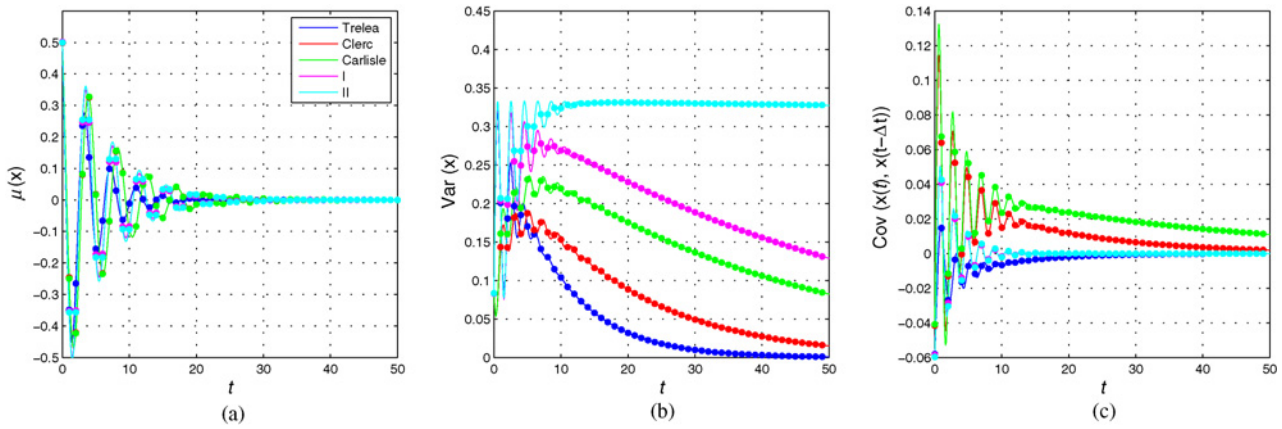

Fig. 8. PSO. (a) Mean, (b) variance, and (c) temporal covariance trajectories for Trelea, Clerc, and Kennedy, and Carlisle and Dozier points, compared to points I and II located on the median line of the first order stability triangle, and on (point I), or close (point II) the border of second order stability for $\alpha = 1$.

points I and II, go to zero faster than those of the Clerc and Kennedy's and Carlisle and Dozier's points. In these two last points the covariance function is almost all the time positive, this meaning that trajectories $x(t-\Delta t)$ and $x(t)$ have a certain degree of similarity.

Fig. 9 shows for the PSO case and $\alpha = 1$ $\left(a_g = a_l\right)$ the maximum variance amplitude and the maximum absolute covariance between $x(t)$ and $x(t-\Delta t)$ affected by its sign

$$\max\left(\left|\mathrm{Cov}\left(x(t), x(t-\Delta t)\right)\right|\right) . \mathrm{sign}\left(\mathrm{Cov}\left(x(t), x(t-\Delta t)\right)\right).$$

Both are deduced numerically using a fine lattice of $\left(\omega, \overline{\phi}\right)$ points located inside the second order stability region. The variance amplitude increases with $\overline{\phi}$, reaching its maximum value in the highest point of the second order stability region, $\left(\omega, \overline{\phi}\right) = (0.42,\ 2.02)$. In this point, the variance stabilizes on 0.497 [Fig. 9(a)]. The temporal covariance [Fig. 9(b)] is almost null close to median line of the first order stability triangle and its minimum negative value is also reached close to the highest point of the second order stability region. In this point the covariance stabilizes on -0.209.

V. Comparison Between the Linear Continuous PSO and GPSO Models and Real Simulations

In this section, we finally show how the linear GPSO approaches the linear PSO continuous model when time step Δt decreases toward zero. It is also important to remark that in the limit, the corresponding GPSO first and second order stability regions tend to those of the continuous PSO. This is done first with the homogeneous systems and after with the transitory solutions, making comparisons with real simulations. This final comparison serves to numerically quantify how these linear models (continuous and discrete) account for the variability observed in real runs. We show that mean trajectories are always very well matched, while the second order moments are only predicted approximately on regions of high variability. Based on the results it is conjectured that nonlinear dependences between the local and global attractors and the trajectories are more important on zones of high variability. We also conclude that the PSO continuous model provides the adequate mathematical model to better understand its discrete counterparts [17].

A. Homogeneous Trajectories

Let us first consider the case where both dynamical systems (continuous and discrete) become homogeneous, i.e., the effect of center of attraction $o(t)$ is not taken into account. Fig. 10 shows the continuous and discrete (GPSO) variance trajectories for two different $\left(\omega, \overline{\phi}\right)$ points on the second order stability region. In Fig. 10(a), we used $\left(\omega, \overline{\phi}\right) = (0.7, 1.7)$ that is located in the eigenvalue complex zone of the corresponding second order stability regions, for both the GPSO and the continuous PSO. It can be observed that both trajectories are of the same kind, and the GPSO variance trajectory approaches the PSO continuous variance as time step goes to zero [Fig. 10(a)–(c)]. Fig. 10(d)–(f) shows the same analysis in the point $\left(\omega, \overline{\phi}\right) = (0.5, 1)$. These dynamics are different, because for $\Delta t = 1$ this point is located on the complex region for the continuous PSO and in the real zigzagging zone for the GPSO. As time step decreases the second order boundary hyperbola goes to infinity and the two dynamics approach each other [Fig. 10(e)], almost overlapping when $\Delta t = 0.1$ [Fig. 10(f)]. Also when Δt decreases, the first and second GPSO zigzagging zones tend to disappear, and the GPSO sampling becomes denser.

Fig. 11 shows the frequency of the homogenous first order trajectories as a function of $\left(\omega, \overline{\phi}\right)$, for the continuous PSO (f_c), and for the GPSO with $\Delta t = 0.1$ (f_{GPSO}). For the continuous PSO, the frequency is related to the imaginary part of the complex eigenvalues, λ_c

$$f_c = \frac{1}{2\pi}\,\mathrm{Im}\left(\lambda_c\right)$$

while in the GPSO case, the frequency is related to the argument of the complex eigenvalues $(\lambda_{\mathrm{GPSO}})$ and Δt as follows:

$$f_{\mathrm{GPSO}}(\Delta t) = \frac{1}{2\pi}\,\frac{\arg\left(\lambda_{\mathrm{GPSO}}\right)}{\Delta t}.$$

Numerically, it can be observed that

$$\lim_{\Delta t \to 0}\ f_{\mathrm{GPSO}}(\Delta t) = f_c.$$

This means that both trajectories have the same frequency content when Δt approaches zero. It can also be shown that the GPSO spectral radius follows the same kind of behavior, i.e., attenuation of trajectories in both cases is very close.

B. Transient Trajectories and Final Discussion

The same analysis has been done with a moving center of attraction using the 1-D Griewank function. The analysis shown here was also performed for other benchmark functions and the results obtained were very similar.

Covariance functions between the oscillation center and the trajectories, needed in $\mathbf{b}_r(t)$ and in $\mathbf{d}_{\mathbf{r}}(t)$ to solve numerically the continuous and GPSO dynamical systems, have been empirically calculated as shown in Section III, devoted to the analysis of the center dynamics. Obviously, the results shown here will be affected by the accuracy of the empirical identification of the center dynamics.

Fig. 12 shows the mean, $E(x(t))$, and the noncentered trajectories, $E\left(x^2(t)\right)$, for the continuous PSO, GPSO with $\Delta t = 0.1$,compared to the corresponding empirical counterparts, for the point $\left(\omega, \overline{\phi}\right) = (-3,\ 3.5)$ located on the real first and second order stability zones. It can be observed that mean trajectories do coincide [Fig. 12(a)]. For the second order trajectories, $E\left(x^2(t)\right)$, the GPSO and PSO homogenous trajectories do coincide [Fig. 12(b)], but they are still far from reality since both go to zero, and the minimum of the cost function is located in $x = 10$. The transient solutions [Fig. 12(c)] show that simulated trajectories are imbedded between those of continuous PSO and GPSO. This example illustrates

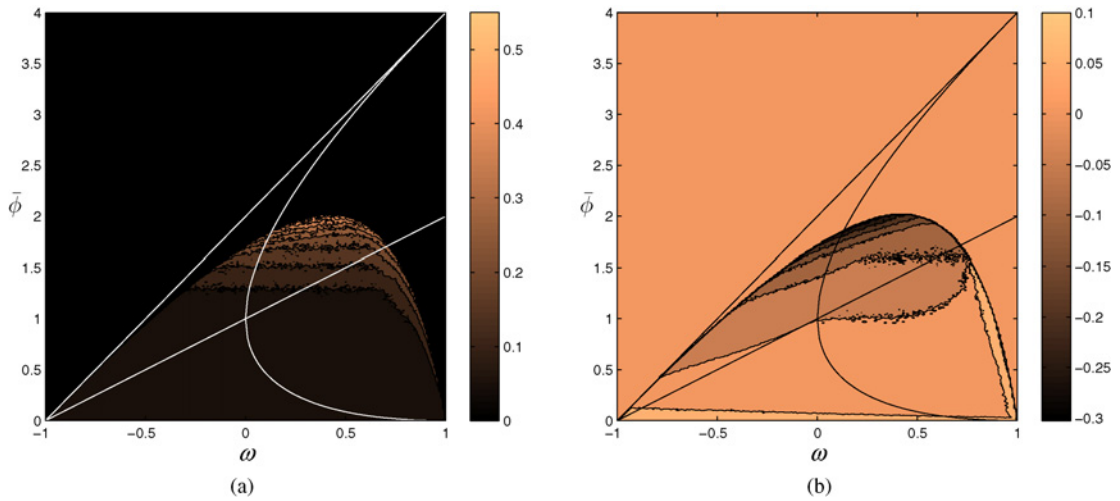

Fig. 9. PSO. (a) Maximum amplitude for the variance trajectories as a function of $(\omega, \overline{\phi})$ for $\alpha = 1$. (b) Maximum absolute covariance $\max(|\mathrm{Cov}(x(t), x(t-\Delta t)|)$, affected by its sign, $\mathrm{sign}(\mathrm{Cov}(x(t), x(t-\Delta t))$.

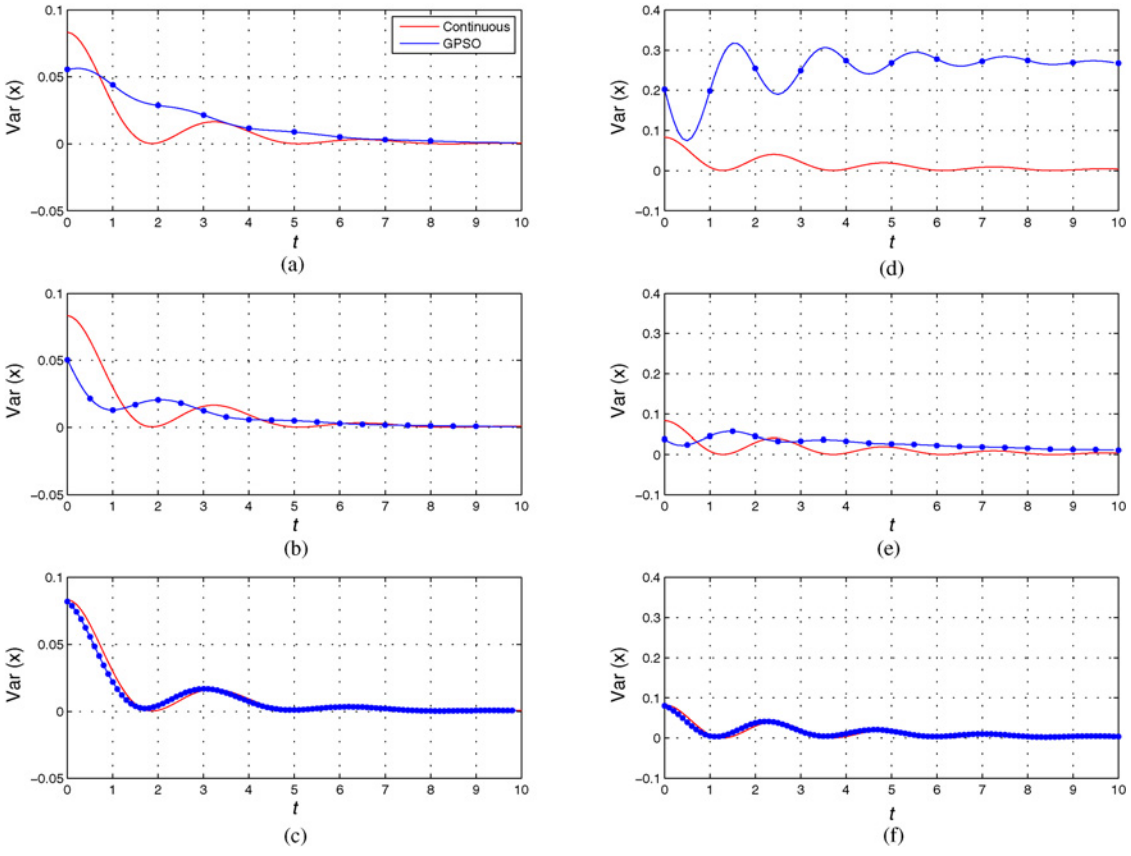

Fig. 10. Numerical convergence of the homogeneous GPSO second order trajectories to the continuous PSO counterparts. (a)–(c) $(\omega, \overline{\phi}) = (0.7, 1.7)$. (d)–(f) $(\omega, \overline{\phi}) = (0.5, 1)$. (a) $\Delta t = 1$. (b) $\Delta t = 0.5$. (c) $\Delta t = 0.1$. (d) $\Delta t = 1$. (e) $\Delta t = 0.5$. (f) $\Delta t = 0.1$.

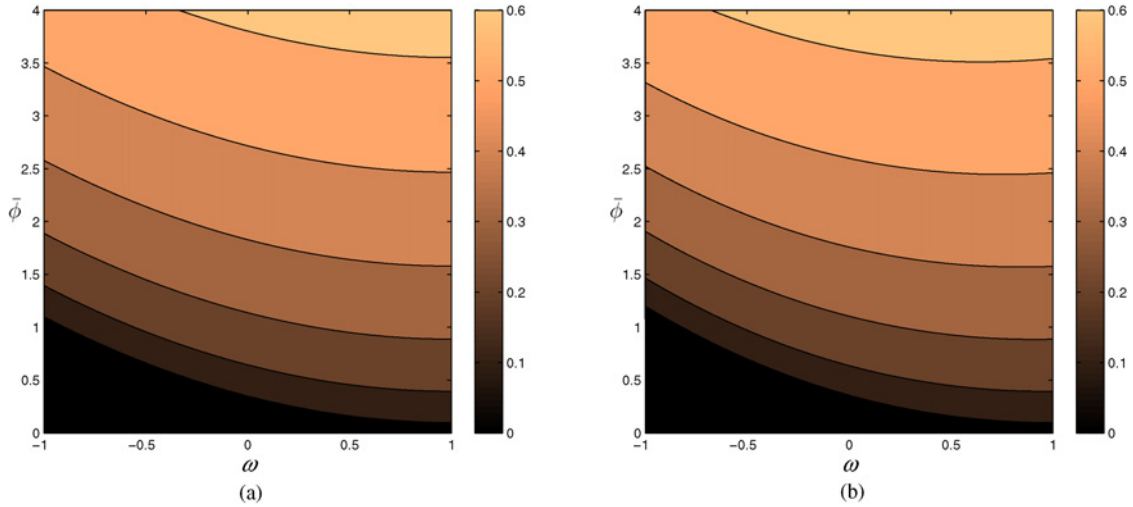

Fig. 11. Frequency of the homogeneous first order trajectories as a function of $(\omega, \bar{\phi})$. (a) Continuous PSO. (b) GPSO with $\Delta t = 0.1$.

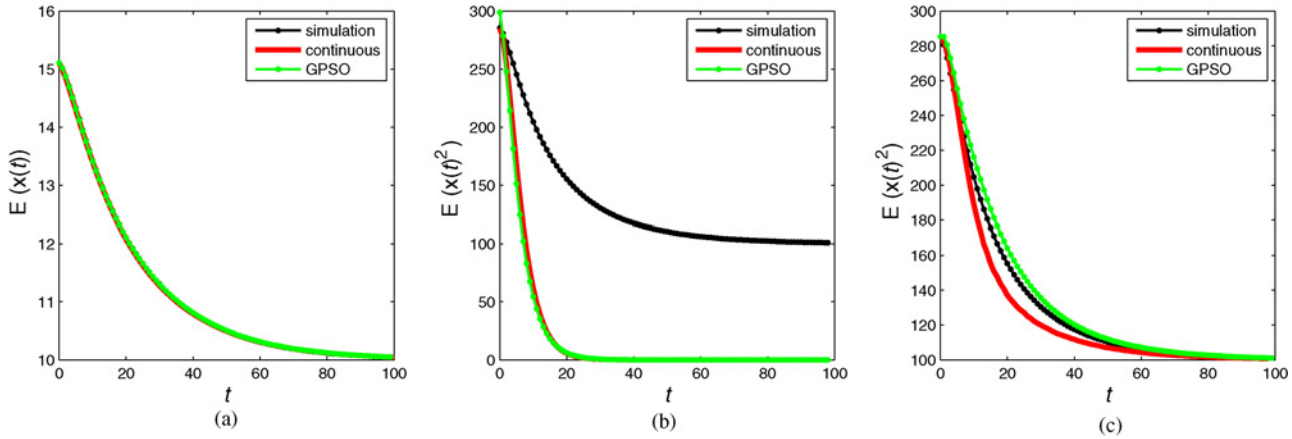

Fig. 12. Mean and noncentered second order moments for the point $(\omega, \bar{\phi}) = (-3, 3.5)$ located on the first and second order real zones of the continuous PSO and GPSO with $\Delta t = 0.1$. (a) Mean trajectories. (b) Homogeneous second order moments. (c) Transient second order moments.

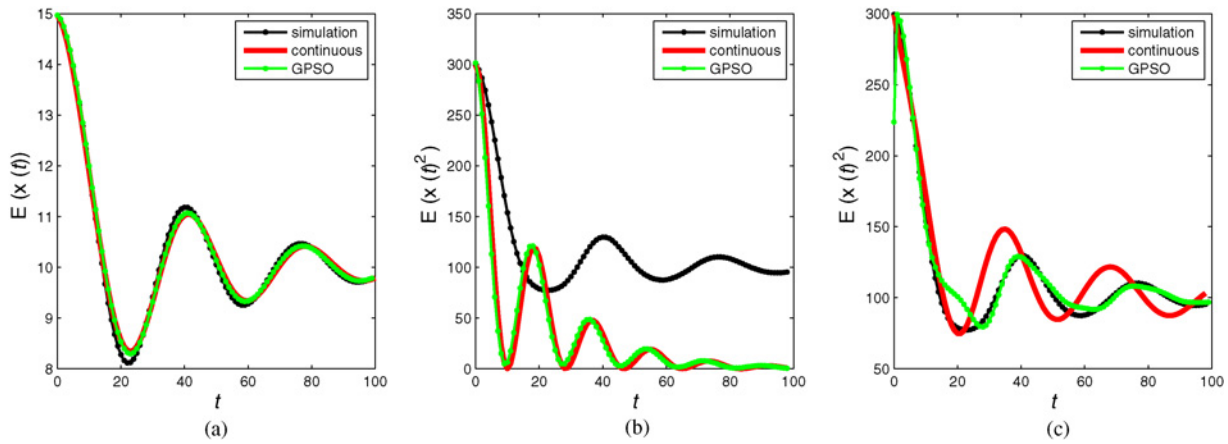

Fig. 13. Mean and noncentered second order moments for the point $\left(\omega, \bar{\phi}\right) = (0.5, 3)$ located on the first and second order complex zones of the continuous PSO and GPSO with $\Delta t = 0.1$. (a) Mean trajectories. (b) Homogeneous second order moments. (c) Transient second order moments.

perfectly the effect of the center of attraction on the second order trajectories.

Fig. 13 shows the same kind numerical experiment for $\left(\omega, \overline{\phi}\right) = (0.5, 3)$ located on the first and second order complex eigenvalue zones, where the first and second order trajectories are oscillatory. It can be observed that mean trajectories are also perfectly matched [Fig. 13(a)]. This can be explained because of the regular behavior of $E\left(o\left(t\right)\right)$ [Figs. 3(a), 4(a), and 5(a)]. The homogeneous $E\left(x^2\left(t\right)\right)$ trajectories for GPSO and continuous PSO are also very close [Fig. 13(b)] but far from real runs for the same reason mentioned above. For the transient solutions [Fig. 13(c)] the results are very sensible to a good identification of the empirical noncentered covariance terms involved in the GPSO and in the continuous PSO. These second terms greatly influence the frequency of the second order trajectories. This identification problem becomes a very difficult task for points located in the second order complex zone [see, for instance, the irregular behavior of $\mathrm{Cov}\left(x'(t), o\left(t\right)\right)$ shown in Fig. 4(d), compared to that shown in Fig. 3(d) for a point in the real zone]. Nevertheless, the GPSO and PSO continuous models are able to describe most of the variability observed in real runs. Also, the same kind of numerical experiments can be done for any particle coordinate using high dimensional benchmark functions. In this case, second order trajectories in the complex zone will show a greater variability than in 1-D, due to the frequency content introduced in $\mathbf{b}_r\left(t\right)$ and $\mathbf{d}_r\left(t\right)$ by the experimental covariance terms.

Finally, it is important to bear in mind that mathematical models are always a simplification of the reality (in this case the behavior of the PSO algorithm applied to real optimization problems), and our major assumption is to model the interaction to the cost function through the covariances functions between the attractors, $l\left(t\right)$, $g(t)$, and the trajectories. Thus, in zones of high variability the linear GPSO and continuous PSO models can only approximately account for the variability (second order moments) observed on the real runs. Nevertheless, as we explained above, the mean trajectories are perfectly matched.

VI. Conclusion

Stochastic analysis of the linear continuous and the generalized PSO models was presented in this paper using the theory of stochastic difference and differential equations for the most general case: transient solutions with a stochastic center of attraction. First and second order moments of the trajectories are, respectively, governed by two systems of first order linear differential equations and linear discrete-time affine dynamical systems. Both models explain the role of the PSO parameters and that of the cost function through the algorithm execution. In the GPSO case, the values of the PSO parameters $\left(\omega, a_g, a_l\right)$ set the isoline of the first and second order spectral radius at execution (exploration and attenuation), and also influence the value of the first and second order forcing terms: the mean trajectory of the center of attraction and the covariance functions between the center of attraction and the trajectories. Analysis of the variance and covariances homogeneous trajectories for the GPSO case completes the studies made in the past for the first order trajectories and serves to explain the similarities and differences between some popular parameter sets found in the literature. Analysis of the oscillation center dynamics for different types of benchmark functions was performed, showing that there was a common behavior for all of them. The analysis of the second order trajectories, together with this last feature, might explain why PSO has been successfully applied to different cost functions considering the same popular PSO parameter sets proposed in the literature.

Finally, a comparison between real simulations, continuous PSO and GPSO models was also shown, when time step is decreasing toward zero. As expected, generalized PSO tends to the continuous PSO when time step approaches zero, and both models account fairly well for the dynamics observed in real runs. Results are excellent when the PSO parameters are chosen on the real zone of the first order stability region. This match worsens for the second order moments when the PSO parameters are chosen on zones of higher variability, nevertheless the first order trajectories are perfectly fitted. This feature might be related to the difficulty of performing a correct identification of the covariances terms involved in our linear models on regions of higher variability.

Up to our knowledge, the analysis presented here constitutes the most realistic attempt to better understand and model the empirical (or real) PSO dynamics.

Acknowledgment

The authors would like to acknowledge Dr. R. Poli, University of Essex, Colchester, Essex, U.K., who suggested a number of fruitful ideas.

Appendix A
Coordinates Interaction for the PSO Continuous Model

Let us call

$$\mathbf{Y}_i\left(t\right) = \begin{pmatrix} x_i\left(t\right) \\ x_i'\left(t\right) \end{pmatrix} \mathbf{Y}_j\left(t\right) = \begin{pmatrix} x_j\left(t\right) \\ x_j'\left(t\right) \end{pmatrix}$$

the vectors describing their position and velocities, and

$$\sigma_{ij}\left(t\right) = \begin{pmatrix} \mathrm{Cov}\left(x_i\left(t\right), x_j\left(t\right)\right) \\ \mathrm{Cov}\left(x_i'\left(t\right), x_j\left(t\right)\right) \\ \mathrm{Cov}\left(x_i\left(t\right), x_j'\left(t\right)\right) \\ \mathrm{Cov}\left(x_i'\left(t\right), x_j'\left(t\right)\right) \end{pmatrix}$$

their corresponding second order moments vector.

Following the same methodology as above, we arrive at the following first order differential system:

$$\begin{aligned} \frac{d\sigma_{ij}\left(t\right)}{dt} &= A_{\sigma_{ij}}\sigma_{ij}\left(t\right) + \mathbf{b}_{\sigma_{ij}}\left(t\right) \\ \sigma_{ij}\left(0\right) &= \sigma_{ijo} \end{aligned} \tag{31}$$

where

$$A_{\sigma_{ij}} = \begin{pmatrix} 0 & 1 & 1 & 0 \\ -\overline{\phi} & \omega - 1 & 0 & 1 \\ -\overline{\phi} & 0 & \omega - 1 & 1 \\ 0 & -\overline{\phi} & -\overline{\phi} & 2(\omega - 1) \end{pmatrix}$$

$$\mathbf{b}_{\sigma_{ij}}(t) = \begin{pmatrix} 0 \\ \overline{\phi}\,\mathrm{Cov}\left(o_i(t), x_j(t)\right) \\ \overline{\phi}\,\mathrm{Cov}\left(x_i(t), o_j(t)\right) \\ \overline{\phi}\left(\mathrm{Cov}\left(x_i'(t), o_j(t)\right) + \mathrm{Cov}\left(x_i'(t), o_j(t)\right)\right) \end{pmatrix}$$

and σ_{ijo} stands for the initial conditions of second order vector $\sigma_{ij}(t)$.

As it occurred for any particle coordinate, the cost function enters in the interaction between coordinates via the covariance functions forming part on $\mathbf{b}_{\sigma_{ij}}(t)$. Obviously, if these similarity functions are zero, the corresponding differential system becomes homogeneous. Also, by means of numerical experiments, covariance functions $\mathrm{Cov}\left(x_i(t), x_j(t)\right)$, $\mathrm{Cov}\left(x_i(t), x_j'(t)\right)$ and $\mathrm{Cov}\left(x_i'(t), x_j'(t)\right)$ turn to be very similar to the functions $\mathrm{Var}(x(t))$, $\mathrm{Cov}\left(x(t), x'(t)\right)$, and $Var\left(x'(t)\right)$, shown in Fig. 2.

The steady regime of (31) is given by

$$\sigma_{ij}\left(t_p\right) = \begin{pmatrix} \mathrm{Cov}\left(x_i'(t_p), o_j(t_p)\right) + \mathrm{Cov}\left(x_j'(t_p), o_i(t_p)\right) \\ -\dfrac{-(\omega-1)\left(\mathrm{Cov}\left(x_i(t_p), o_j(t_p)\right) + \mathrm{Cov}\left(x_j(t_p), o_i(t_p)\right)\right)}{2(\omega-1)} \\ \dfrac{\left(\mathrm{Cov}\left(x_i(t_p), o_j(t_p)\right) - \mathrm{Cov}\left(x_j(t_p), o_i(t_p)\right)\right)\overline{\phi}}{2(\omega-1)} \\ \dfrac{\left(\mathrm{Cov}\left(x_j(t_p), o_i(t_p)\right) - \mathrm{Cov}\left(x_i(t_p), o_j(t_p)\right)\right)\overline{\phi}}{2(\omega-1)} \\ -\dfrac{\left(\mathrm{Cov}\left(x_i'(t_p), o_j(t_p)\right) + \mathrm{Cov}\left(x_j'(t_p), o_i(t_p)\right)\right)\overline{\phi}}{2(\omega-1)} \end{pmatrix}$$

which obviously depends on the above mentioned covariance values at t_p.

Appendix B
Coordinates Interaction for the GPSO Case

Let us call $x_i(t)$, $x_j(t)$ both coordinates fulfilling the difference equations

$$x_i(t+\Delta t) - Ax_i(t) - Bx_i(t-\Delta t) = C_i(t) \quad t,\ \Delta t \in R$$

$$x_j(t+\Delta t) - Ax_j(t) - Bx_j(t-\Delta t) = C_j(t) \quad t,\ \Delta t \in R.$$

Let us call

$$\mathbf{r}_{ij}(t) = \begin{pmatrix} E\left(x_i(t)\,x_j(t)\right) \\ E\left(x_i(t-\Delta t)\,x_j(t)\right) \\ E\left(x_i(t)\,x_j(t-\Delta t)\right) \\ E\left(x_i(t-\Delta t)\,x_j(t-\Delta t)\right) \end{pmatrix}.$$

The following relationships apply:

$$E\left(C_i(t)\,x_j(t)\right) = \overline{\phi}\Delta t^2 E\left(o_i(t)\,x_j(t)\right)$$

$$\begin{aligned} E\left(x_i(t+\Delta t)x_j(t)\right) &= E(A)\,E\left(x_i(t)x_j(t)\right) \\ &\quad + BE\left(x_i(t-\Delta t)x_j(t)\right) + E\left(C_i(t)\,x_j(t)\right) \\ &== E(A)\,E\left(x_i(t)x_j(t)\right) \\ &\quad + BE\left(x_i(t-\Delta t)x_j(t)\right) \\ &\quad + \overline{\phi}\Delta t^2 E\left(o_i(t)\,x_j(t)\right) \end{aligned}$$

$$\begin{aligned} E\left(x_i(t+\Delta t)x_j(t+\Delta t)\right) &= E\left(A^2\right)E\left(x_i(t)x_j(t)\right) \\ &\quad + BE(A)\,E\left(x_i(t-\Delta t)x_j(t)\right) \\ &\quad + + E\left(AC_i(t)\,x_j(t)\right) \\ &\quad + BE(A)\,E\left(x_i(t)x_j(t-\Delta t)\right) + \\ &\quad + B^2 E\left(x_i(t-\Delta t)x_j(t-\Delta t)\right) \\ &\quad + BE\left(C_i(t)\,x_j(t-\Delta t)\right) + \\ &\quad + E\left(Ax_i(t)\,C_j(t)\right) \\ &\quad + BE\left(x_i(t-\Delta t)C_j(t)\right) \\ &\quad + E\left(C_i(t)\,C_j(t)\right). \end{aligned}$$

Then, $\mathbf{r}_{ij}(t)$ follows the following second order affine dynamical system:

$$\mathbf{r}_{ij}(t+\Delta t) = A_{ij}\mathbf{r}_{ij}(t) + \mathbf{d_{ij}}(t)$$

where

$$A_{ij} = \begin{pmatrix} E\left(A^2\right) & BE(A) & BE(A) & B^2 \\ E(A) & 0 & B & 0 \\ E(A) & B & 0 & 0 \\ 1 & 0 & 0 & 0 \end{pmatrix}$$

$$\mathbf{d_{ij}}(t) = \begin{pmatrix} d_1 \\ \overline{\phi}\Delta t^2 E\left(x_i(t), o_j(t)\right) \\ \overline{\phi}\Delta t^2 E\left(x_j(t), o_i(t)\right) \\ 0 \end{pmatrix}$$

being

$$\begin{aligned} d_1 &= E\left(AC_i(t)\,x_j(t)\right) + BE\left(C_i(t)\,x_j(t-\Delta t)\right) + \\ &\quad + E\left(AC_j(t)\,x_i(t)\right) + BE\left(C_j(t)\,x_i(t-\Delta t)\right) \\ &\quad + E\left(C_i(t)C_j(t)\right) \end{aligned}$$

where the term $E\left(C_i(t)C_j(t)\right)$ involves the correlation between the attractors of both particles.

These moments can also be centered, as we did for the GPSO second order moments. It can be probed numerically that $E\left(x_i(t)\,x_j(t)\right)$ and $E\left(x_i(t-\Delta t)\,x_j(t)\right)$ trajectories are similar to $E\left(x^2(t)\right)$ and $E\left(x(t-\Delta t)\,x(t)\right)$.

References

[1] E. Ozcan and C. K. Mohan, "Analysis of a simple particle swarm optimization system," in *Proc. ANNIE*, vol. 8. Oct. 1998, pp. 253–258.

[2] E. Ozcan and C. K. Mohan, "Particle swarm optimization: Surfing the waves," in *Proc. IEEE CEC*, vol. 3. Jul. 1999, pp. 1939–1944.

[3] A. Carlisle and G. Dozier, "An off-the-shelf PSO," in *Proc. Part. Swarm Optimization Workshop*, Apr. 2001, pp. 1–6.

[4] M. Clerc and J. Kennedy, "The particle swarm: Explosion, stability, and convergence in a multidimensional complex space," *IEEE Trans. Evol. Comput.*, vol. 6, no. 1, pp. 58–73, Feb. 2002.

[5] I. C. Trelea, "The particle swarm optimization algorithm: Convergence analysis and parameter selection," *Infor. Process. Lett.*, vol. 85, pp. 317–325, Mar. 2003.
[6] Y.-L. Zheng, L.-H. Ma, L.-Y. Zhang, and J.-X. Qian, "On the convergence analysis and parameter selection in particle swarm optimization," in *Proc. 2nd ICMLC*, vol. 3. Nov. 2003, pp. 1802–1807.
[7] F. van den Bergh and A. P. Engelbrecht, "A study of particle swarm optimization particle trajectories," *Inform. Sci.*, vol. 176, pp. 937–971, Apr. 2006.
[8] J. L. Fernández-Martínez, E. García-Gonzalo, and J. P. Fernández-Alvarez, "Theoretical analysis of particle swarm trajectories through a mechanical analogy," *Int. J. Comput. Intel. Res.*, vol. 4, no. 2, pp. 93–104, 2008.
[9] B. Brandstätter and U. Baumgartner, "Particle swarm optimization: Mass-spring system analogon," *IEEE Trans. Magnet.*, vol. 38, no. 2, pp. 997–1000, Mar. 2002.
[10] S. M. Mikki and A. A. Kishk, "Physical theory for particle swarm optimization," *Prog. Electromagnetics Res.*, vol. 75, pp. 171–207, 2007.
[11] M. Clerc, "Stagnation analysis in particle swarm optimization or what happens when nothing happens," Dept. Comput. Sci., Univ. Essex, Colchester, U.K., Tech. Rep. CSM-460, Aug. 2006.
[12] V. Kadirkamanathan, K. Selvarajah, and P. J. Fleming, "Stability analysis of the particle dynamics in particle swarm optimizer," *IEEE Trans. Evol. Comput.*, vol. 10, no. 3, pp. 245–255, Jun. 2006.
[13] M. Jiang, Y. P. Luo, and S. Y. Yang, "Stochastic convergence analysis and parameter selection of the standard particle swarm optimization algorithm," *Inform. Process. Lett.*, vol. 102, pp. 8–16, Apr. 2007.
[14] R. Poli and D. Broomhead, "Exact analysis of the sampling distribution for the canonical particle swarm optimizer and its convergence during stagnation," in *Proc. 9th GECCO*, 2007, pp. 134–141.
[15] R. Poli, "Dynamics and stability of the sampling distribution of particle swarm optimizers via moment analysis," *J. Artif. Evol. Appl.*, vol. 2008, no. 761459, p. 10, Jan. 2008.
[16] J. L. Fernández-Martínez and E. García-Gonzalo, "The generalized PSO: A new door for PSO evolution," *J. Artif. Evol. Appl.*, vol. 2008, no. 861275, p. 15, Jan. 2008.
[17] J. L. Fernández-Martínez and E. García-Gonzalo, "The PSO family: Deduction, stochastic analysis and comparison," *Swarm Intell.*, vol. 3, pp. 245–273, Dec. 2009.
[18] R. Poli, "Analysis of the publications on the applications of particle swarm optimization," *J. Artif. Evol. Appl.*, vol. 2008, no. 685175, p. 10, Jan. 2008.
[19] J. Q. Sun, *Stochastic Dynamics and Control*. Amsterdam, The Netherlands: Elsevier, 2006.
[20] L. D. Lutes and S. Sarkani, *Random Vibrations. Analysis of Structural and Mechanical Systems*. Amsterdam, The Netherlands: Elsevier, 2004.
[21] M. Clerc, "The swarm and the queen: Toward a deterministic and adaptive particle swarm optimization," in *Proc. CEC*, vol. 3. 1999, pp. 1951–1957.
[22] P. N. Suganthan, N. Hansen, J. J. Liang, K. Deb, Y. P. Chen, A. Auger, and S. Tiwari, "Problem definitions and evaluation criteria for the CEC 2005 special session on real parameter optimization," Nanyang Technol. Univ., Singapore, and Kangal, Kanpur Genetic Algorithms Lab., IIT, Tech. Rep., Kanpur, India, Tech. Rep. 2005005, May 2005.

Juan Luis Fernández-Martínez received the graduate degree, and the Ph.D. degree in 1994, both in mining engineering from the University of Oviedo, Oviedo, Spain.

He was a Petroleum Engineer with École Nationale du Pétrole et des Moteurs, Paris, France, in 1988, and with the Royal School of Mines, Imperial College, London, U.K., in 1989. After working as a Computing and Consulting Engineer in France for a few years in the petroleum industry, he joined the Department of Mathematics, University of Oviedo, in 1994, where he is currently a Professor of Applied Mathematics. He works on inverse problems and stochastic optimization. From 2008 to 2010, he was a Visiting Professor with the Department of Civil and Environmental Engineering, University of California Berkeley, Berkeley, and with the Department of Energy Resources, Stanford University, Palo Alto, CA, where he worked on inverse problems and uncertainty quantification applied to reservoir optimization.

Esperanza García-Gonzalo received the Bachelor's degree in mining engineering from the University of Oviedo, Oviedo, Spain, in 1990.

Since 1990, she has been an Associate Professor with the Department of Mathematics, University of Oviedo. Her current research interests include global stochastic optimization methods, particularly particle swarm optimization and differential evolution, and their application to inverse problems in geophysics and reservoir engineering.